JPRS-UEQ-90-002
6 FEBRUARY 1990

JPRS Report

Science & Technology

USSR: Engineering & Equipment

Science & Technology
USSR: Engineering & Equipment

JPRS-UEQ-90-002 *6 February 1990*

CONTENTS

UDC 621.315.592:772.99

Kinoforms: Technologies, New Components and Optical Systems; Part I

907F0056A Novosibirsk AVTOMETRIYA No 3 May-Jun 89 pp 95-102

[First part of article under the "Components of Photonic Systems" rubric by V. P. Korolkov, V. P. Koronkevich, I. A. Mikhaltsova, I. G. Palchikova, A. G. Poleshchuk, A. G. Sedukhin, A. P. Sokolov, Ye. G. Churin, and Yu. I. Yurlov, Novosibirsk]

[Text] The first results from investigations of a new phototechnology for synthesis of kinoform optical components are presented in [1]. To record the diffraction structure, a laser beam focused to the dimensions of a wave length is used as the primary "tool" of a computer-controlled precision photoplotter. This method of production of the component resembles the techniques of the pointillist painters. The structure of the picture is formed by a superpositioning of spots and circular arcs. The space frequency of the "pattern" may reach to 1500 mm^{-1} or more. A recording frequency suitable for practical purposes can be achieved when working in a polar coordinate system. The photoplotter which we have developed [2-4] makes it possible to prepare the amplitude mask of the component (stencil), the topology of which is then transferred to glass by photolithography.

The current article presents new methods and procedures for production of kinoform components of any desired topology and profile, along with results from the investigation of new materials for production of masking coatings of the stencils. The main attention is given to extended zone plates [5, 6], in which the lengthwise and transverse dimensions of the caustic near the focus are not so strictly correlated as in the case of a lens with good convergence. In bifocus microscopes [7], devices for putting out images from computer [8], and laser technological layouts, components are needed which lengthen the caustic while retaining the projective properties of the optical system.

In data recording and playback disks [9], motion sensors working by the principle of triangulation [10], and devices for creation of a reference light line [1], components are needed which display a spot of light at the entrance in the form of a line segment, situated along the optical axis. The performance of projective transformations is obligatory in these instances. The conventional optical components can seldom control the caustic effectively, and therefore a solution may be found in the combination of kinoform and conventional components.

A number of new optical components have been synthesized with a transformed caustic. Among these are the axicon, coupled with a Siemens plate or lens; a lens with improved focusing depth; half-tone scales with diffraction gradations, capable of optical cross coupling. These components combine the functions of two or more elements and allow a substantial simplification of the design of the optical instrument. The practical part of the article presents results from investigation of several layouts of new instruments with diffractions components.

I. New technologies. *Formation of images of arbitrary topology.* Refer to the setup in Fig. 1. This shows, in simplified form, the basic elements of a laser photoplotter, working in a polar coordinate system. The image is constructed by the focused laser beam on a substrate 1 with light-sensitive film. The substrate is secured to a faceplate in a spindle 2. The angular position of the substrate when turned by a motor is fixed on a circular scale 3 by photoelectric sensors 4 and 5. The increment of determination of the angular position is 1 second.

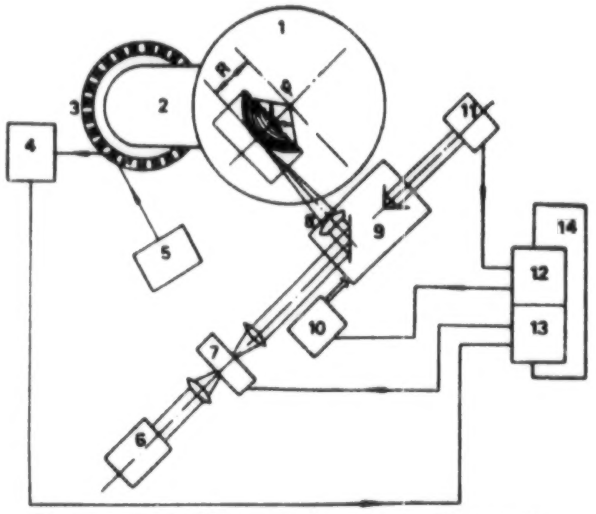

Figure 1. Block Diagram of the Laser Photoplotter

The optical arrangement of the setup includes an argon laser 6, a modulator 7, and a focusing microlens 8. The microlens is fastened to a movable carriage 9, which travels along the radius by a linear motor 10. The position is checked by laser interferometer 11. The linear motor and interferometer are linked to an electronic assembly 12, in which signals are put out to control the movement. The smallest increment of movement is $\lambda/8$ (around 0.079 μm). Registration in an angle can be done by sending signals (turn on and off) to the acousto-optical modulator 7 from the control unit 13. Information as to the angular position of the substrate is sent to 13 from the angle-code sensor 3-5. Control and monitoring of the working of all components are exercised by computer 14.

In [1] it is shown that the photoplotter is especially convenient for registration of circular structures of the zone plate type, when the recording is continuous in amplitude and discrete in the radial direction. During the registration, the controlling computer turns on the modulator for the time of one rotation of the spindle and the laser beam with specified power exposes a circle on

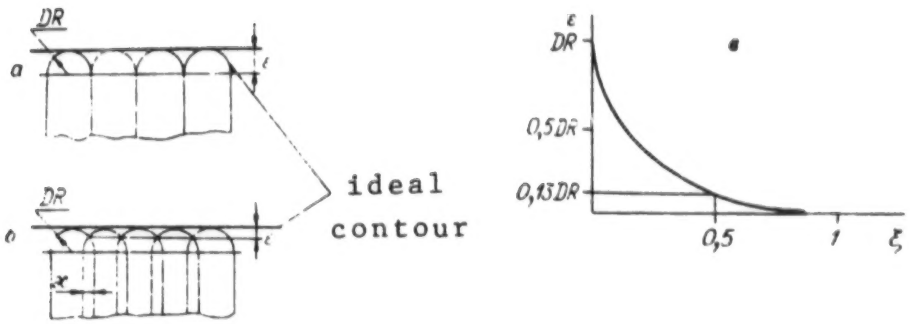

Figure 2. Traces of the Laser Beam on Material: a - Image Without Overlap; b - With Overlap of κ; c - Edge Irregularity ε as Function of Degree of Overlap ξ.

the light-sensitive material. Later on, at a command from the computer, the carriage with microlens is moved and the recording process repeats.

For synthesis of arbitrary images, the registration must also be discrete in amplitude. Figure 1 shows schematically the traces of the laser beam during the construction of a square, arranged nonsymmetrically with respect to the axis of rotation of the substrate. The field of the image is filled with circular arcs. For images with high space frequency, the arcs are contracted into points.

The spatial resolution of the photoplotter lies in the range of 0.7-1 μm and is determined by the dimension of the focal spot and the properties of the light-sensitive material. The irregularities of the edge of the synthesized image depend on the degree of overlap of the tracks, the size of the light spot, and the shape of the image fragment. Figure 2 a-c shows the relationship for the irregularity of the edge $\varepsilon = DR(1 - \sqrt{2\xi(1-\xi/2)})$ as a function of the radius of the spot DR and the relative overlap $\xi=\kappa/(2DR)$. Here, κ is the absolute overlap of tracks. The permissible level of irregularity depends on the requirements for image quality.

The process of production of images in the photoplotter consists of two stages: preparation of the data and construction of the image proper. The division into two stages makes it possible to lessen the temperature, mechanical, and electrical drift of the system.

In the data preparation, the problem of finding the points of intersection of a circle of radius R with the contour of the image being synthesized is solved. The angular coordinates corresponding to the ends of the circular arc along which the exposure is made are determined. For a diameter of spot of 1 μm and azimuth increment of 1 second, the volume of initial data needed to construct a grid of dimension 1x1 cm^2, consisting of 1000 rectangles, is 50 Mbyte. The data preparation involves great expenditure of time and therefore is done as a separate step, prior to the image synthesis. During fabrication of the component, the task is to read, transmit, and process data concerning the angular and radial coordinates and to control in real time the displacement of the carriage and the modulator of the laser beam. As an example, Fig. 3 shows fragments of images that have been synthesized.

The first fragment (Fig. 3a) shows the topology of the amplitude mask for a new component which combines in itself a reflecting mirror and a focusing lens. The mirror is placed at an angle of 45° to the incident beam. The memory volume for preparation of the ellipse registration data is 20 Mbyte. To calculate these, 10 hours of machine time of the Elektronika 79 computer were needed. The time to make the mask was 5 h (control computer SM-4).

Figure 3b shows a special scale. The scale factor is 10 μm, the width of the ruling is 5 μm, and the length of the ruling is 30 μm. The overall length of the scale is 5 mm. The scale is intersected by five concentric circles, arranged every 1 mm, and six circles every 2.5 mm. The scale errors lie in the range of 1 μm. Figure 3c shows fragments of the service text that usually accompanies the synthesized mask pattern.

Methods of production of surface microrelief. Kinoform optical elements with the required modulation phase function can be made by altering the depth of the surface relief or the coefficient of refraction of the substrate material [1].

The technology for production of a phase relief, based on methods of photolithography, requires construction of a set of photomasks, the pattern of which is consecutively converted into separate steps in the substrate material. However, the resolving capacity (1-2.5 μm), which is limited by the process equipment used, and the accuracy of alignment of the masks (0.5-1 μm) do not allow fabrication of lenses with large apertures and high (70-80%) diffraction efficiency [11]. The phase profile of a kinoform can also be produced by a single "half-tone" photomask. After exposure and development of the photoresist in the layer, a relief is formed with depth proportional to the transmission function of the mask. This relief is subsequently transferred to the substrate material by ionic etching. The main stages of this technological process are shown in Fig. 4.

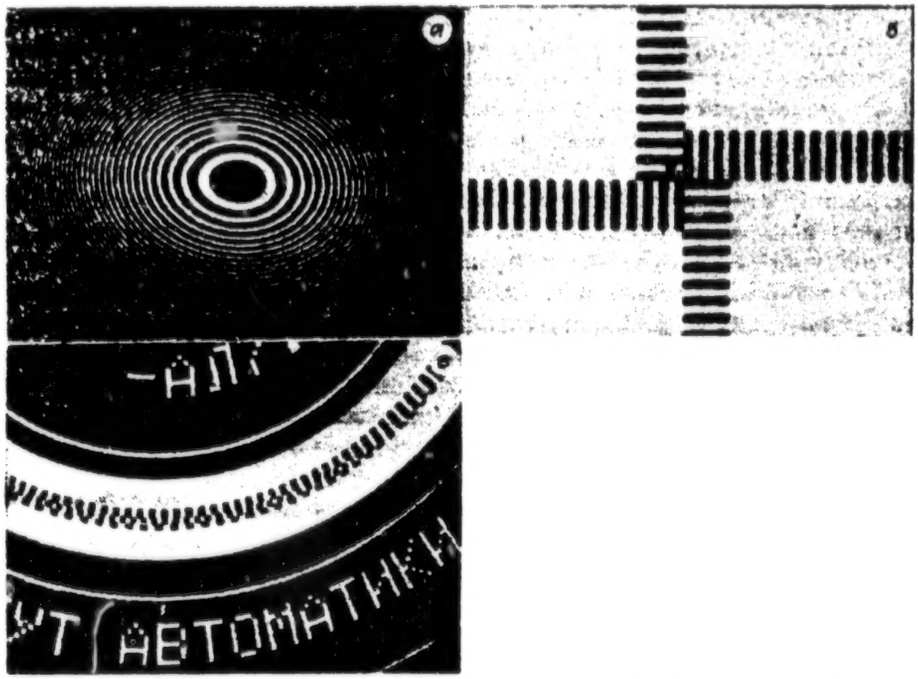

Figure 3. Fragments of Images of Nonsymmetrical Structures: a - Elliptical Zone Plate (number of zones 500, diameter of component 40 mm); b - Ruled Scale; c - Service Text

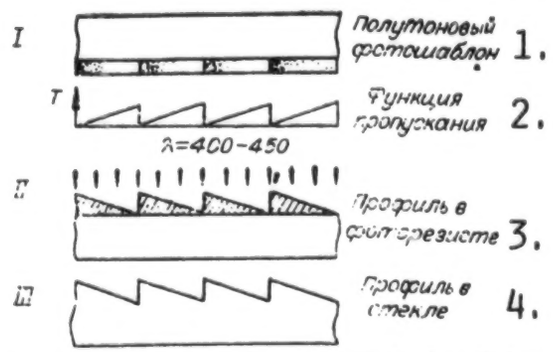

Figure 4. Phase Profile Production Technology Using a Half-Tone Photomask: I - Preparation of Photomask; II - Exposure and Development of Photoresist; III - "Dry" Etching of Glass.

Key: 1. Half-tone photomask 2. Transmission function 3. Profile in photoresist 4. Profile in glass

On the one hand, this method greatly simplifies the fabrication process, since there is no need to line up a group of photomasks or repeatedly etch the substrate material, but on the other hand it is necessary to prepare a mask with given transmission, varying by a sawtooth or other more complicated law. Photoemulsions may be used for these purposes only when making kinoform elements with zones at least 50-100 μm wide. The nonlinearity of the γ-characteristic, the considerable thickness of the layer (several micrometers), and the presence of grains prevent the making of emulsion half-tone photomasks for kinoforms of considerable aperture ratio. Two methods are presented below for production of a surface microrelief that are free from these drawbacks.

1. HALF-TONE REGISTRATION IN THE MASK MATERIAL. A promising material for fabrication of a mask coating of photomasks is amorphous silicon a- Si. Half-tone and binary microimages with high spatial resolution can be produced on thin silicon films (around 100 nm).

Optical registration on a-Si films is based on a solid state transition from the amorphous to the polycrystalline state, realized under local heating by laser beam [12]. This transition is accompanied by a decrease in the coefficient of absorption α and a rise in the coefficient of

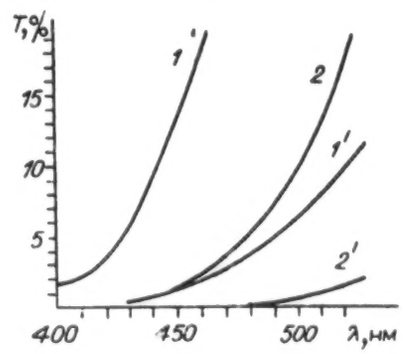

Figure 5. Transmission Spectra T for Silicon Films. Abscissa, Nanometers.

transmission T. Under the action of the radiation, the film becomes antireflecting. The pattern of the photomask is obtained directly in the process of registration with no later chemical treatment.

Figure 5 shows the variation in the transmission spectrum T for films of thickness 100 (1, 1') and 200 (2, 2') nm (1' and 2' are the spectra before, 1 and 2 the spectra after exposure to the radiation). Since the microimage of the photomask is transferred to the photoresist during the subsequent steps, we are mainly concerned with the spectral range of 400-450 nm, where the photoresist is most sensitive to light. At wavelength of 440 nm, both the sensitivity of the resist and the transmission T_{pc} of the irradiated polycrystalline sectors of the photomask are quite high. Since the image contrast (the ratio T_{pc}/T_a, where T_a is the transmission of the nonirradiated film) grows with increasing thickness of the film, while the transmission T_{pc} decreases, the film thickness of 100 nm is optimal for binary masks. The contrast in this case is 10, while the transmission factor is T_{pc}=9% (see Fig. 5). Figure 6 shows the contrast as function of the power of the writing beam at different scanning rates. On the whole, the variation in the image contrast is quite linear. Thus, half-tone optical registration is possible in a certain range of power variation. When copying half-tone photomasks it is necessary to work on the linear segment of the characteristic curve of the photoresist, and therefore the maximum contrast should lie in the range of 4-10. Consequently, for half-tone photomasks the film thickness may be decreased to 60-80 nm, in order to boost the transmission of the antireflecting portion.

Optical registration on silicon films is distinguished by high spatial resolution. Figure 7 shows a microphotograph of groups of lines registered by laser beam of diameter 0.8 μm at scanning rate of 100 cm/s. The distance between the lines (the period) lies in the range of 0.48-1 μm. The width of the tracks formed is 0.25-0.3 μm for scanning rates above 10 cm/s and beam power below the melting threshold P_0. When the beam power is $P>P_0$, the width increases to 0.6-0.8 μm. When the rate

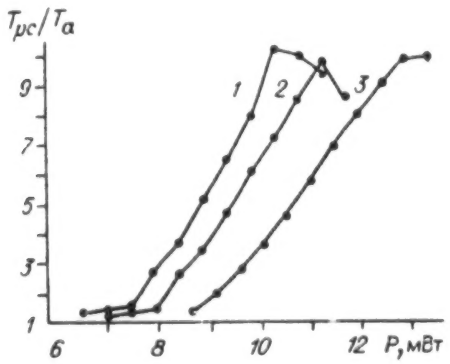

Figure 6. Writing Contrast T_{pc}/T_a as Function of Laser Beam Power (in mW) at Scanning Rates of 49 (1), 82 (2), and 140 cm/s (3).

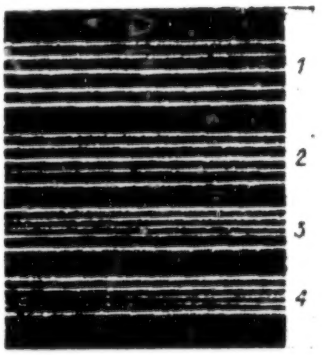

Figure 7. Microphotograph of Groups of Lines Registered With Period (m) of: 1 - 1; 2 - 0.79; 3 - 0.63; 4 - 0.48

is lowered to 10^{-2} cm/s, the width of the tracks monotonically increases to 0.4-0.5 μm. The achievement of high spatial resolution in a broad range of scanning speeds is evidently due to several factors involving the thermal nature of the registration process. First, there is a strong nonlinear relationship between the crystallization process and the temperature; second, films of amorphous silicon have low thermal conductance (around $2x10^{-2}$ W/cmK); third, because of the translucency of the film at thicknesses of around 100 nm, the energy absorption in the central portion of the gaussian beam is substantially lessened, which results in localization of structural changes in a small region.

Calculations of the optical transmission and reflection constants of the films indicate that the coefficient of absorption α decreases monotonically with rising beam power. An investigation of the structural changes by the technique of Raman scattering spectroscopy has confirmed that crystallization of the film takes place under the action of the laser light. The half-tone recording effect depends on the buildup of the overall volume of microcrystals in the specimen and is little dependent on their size.

Let us mention the primary characteristics of photomasks with silicon masking layer:

the production of the microimage on the masking layer occurs by virtue of the translucency of the film under the action of the focused laser beam; no subsequent chemical treatment of the mask is required;

the coating material enables high spatial resolution, reaching 0.25-0.30 μm; even at low registration speeds, this amounts to 1000 line/mm;

the amorphous and polycrystalline states of silicon are stable over time and guarantee reproducibility when making copies.

Among the drawbacks should be mentioned the poor transmission of the translucent areas of the film in the region of sensitivity of the photoresists (< 450 nm), which leads to longer exposures when transferring the mask pattern to the photoresist.

2. THE PHOTOSCREEN METHOD OF PRODUCTION OF A MICRORELIEF. The technological process shown in Fig. 4 can also be realized with the use of conventional masking layers based on chromium or iron oxide, which provide only a two-gradation transmission [13]. Digitization of the original half-tone transmission function S(x) of the photomask is done by screening, while the projection optical system that plays the part of a filter of space frequencies (Fig. 8a) reconstructs, in the plane of the registering material, the distribution of intensity in proportion to the original half-tone function (Fig. 8b). After exposure and development, a relief is formed in the photoresist layer, which is transferred by ionic etching to the substrate material with specified scale.

The screening period of the mask is chosen from the condition $t_p<2\pi/\omega_{max}$, where ω_{max} is the maximum space frequency of transmission of the optical system (limit of resolution). The width of the screen lines is $l=t_pS(x)$. If the original half-tone transmission function (with period t) is represented as a Fourier series:

$$S(x) = A_0/2 + \sum_{k=1}^{\infty} b_k \sin k\Omega x$$

(where for a sawtooth profile $A_0=1$, $b_k=2/\pi k$), then it can be shown that the distribution of intensity of light passing through the mask in the plane of the photoresist has the form:

$$I_\Phi(x) = \frac{A_0}{2} + \sum_{k=1}^{K} b_k M\left(\frac{k\Omega}{\omega_{max}}\right)\sin k\Omega x +$$

$$\frac{1}{\pi}\sum_{k=1}^{K}\sum_{n=1}^{\infty}\sum_{m=-\infty}^{\infty}\frac{1}{n}J_m[\pi n b_k(-1)^{k+1}]\times$$

$$\times[(-1)^{k+1} - (-1)^{k+m+n+1}]M$$

$$\left(\frac{km\Omega + n\omega_0}{\omega_{max}}\right)\sin\left[(km\Omega + n\omega_0)x + A_0 n\frac{\pi}{2}\right].$$

Here, $\Omega = 2\pi/t$, $\omega = 2\pi/t_p$, and $M(\omega/\omega_{max})$ is the optical transmission function (OTF) of the projection system. The distribution contains, in addition to the original function (first two terms), the combination noise components occasioned by the screening. Proper choice of the magnitudes of t_p, ω_{max}, $M(\omega/\omega_{max})$, and the depth of modulation S(x) makes it possible to reduce the level of

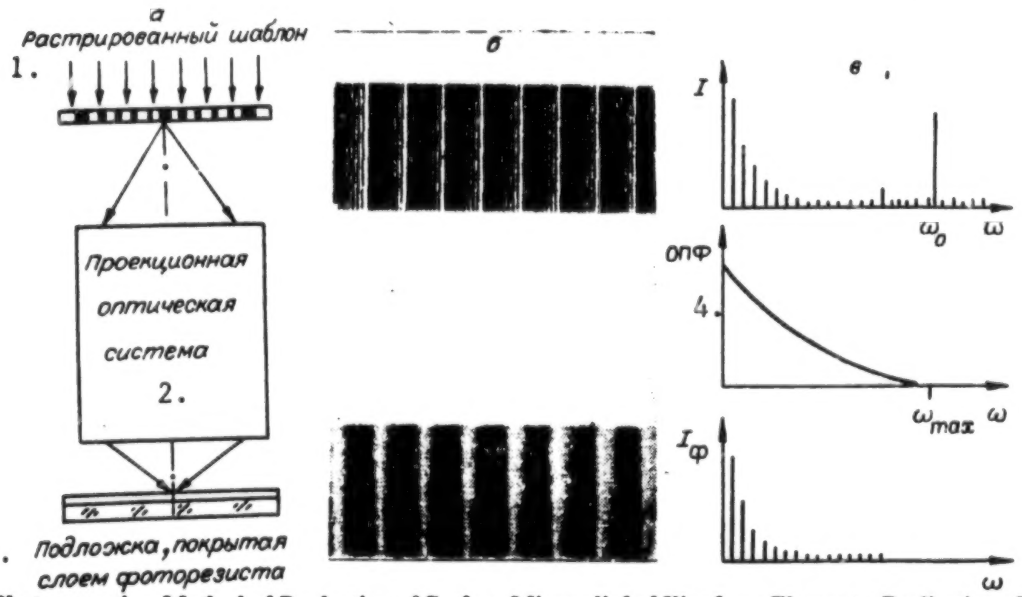

Figure 8. Photoscreening Method of Production of Surface Microrelief of Kinoform Elements. Realization of the Proposed Technique by Means of a Projection Photolithography Device (a); Fragment of the Scanned Photomask (t_p=6, l_{min}=1.2 μm) and Distribution of Intensity Reconstructed in Plane of the Photoresist (b); Spectrum of Space Frequencies of Mask (t=10, t_p=0.6 μm) and Result of Filtration of Step-and-Repeat Camera by Optical System (c).

Key: 1. Scanned mask 2. Projection optical system 3. Substrate coated with photoresist layer 4. OTF

these components to an acceptable value, as shown in Fig. 8c.

The diffraction efficiency η of the kinoforms synthesized by the given technique is determined mainly by the amount of exposure and the number $K=\omega_{max}/\Omega-1$ of space harmonics forming the distribution of the intensity in the plane of the photoresist. The value of η varies from 0.33 (when K=1) to 1 (when K approaches infinity). Figure 9 shows the change in the diffraction efficiency of a kinoform synthesized by means of screen techniques (a) as a function of the number of harmonics and, for comparison, one made by the conventional technology (b) as function of the number of steps. The curve b was computed for the ideal case when there are no process mistakes in production of the structure (errors of alignment, errors of production of the width and depth of the steps, the etching wedge, etc.). In practice, the value of η is much lower for elements with dimension of zones on the order of 10 μm or less. In the photoscreen method, this source of errors is absent. Therefore, by using the projection system of an ordinary step- and-repeat camera (for example, the lens UMVV 1:10/0.35 of the Carl Zeiss company has a spatial resolution better than 1500 mm^{-1}), it is easy to obtain a diffraction efficiency of kinoforms on the order of 80% for a zone dimension of 5-8 μm (in this case, K=8- 10).

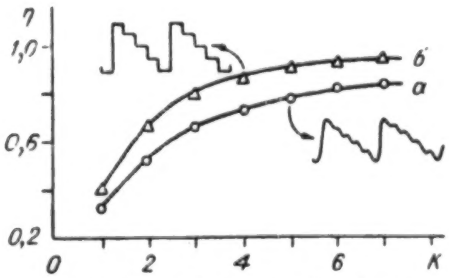

Figure 9. Diffraction Efficiency of Kinoforms Synthesized by Photoscreening (a) and Photolithography (b) Techniques

The possibility of making kinoform lenses and aberration correctors was experimentally investigated. A relief was formed with periodic, linearly increasing and parabolic forms, having a maximum depth of 1.2 μm and minimum period of 5 μm. The photomasks (magnified tenfold, t_p=6 μm, l=1-8 μm) were prepared in chromium films by the thermochemical technique. Exposure of the photoresist layer (AS- 1450) was done in a projection photolithography layout with tenfold reduction. The diffraction efficiency of certain of the resulting lenses (focal distance 25 mm, diameter 5 mm) reached 0.85, which is near the theoretical limit for K=8-9. As many as 50 identical elements were made on a single 102x102x2.5 mm sheet. The diffraction efficiency of the correctors lay in the range of 0.5-0.85 and depended on the exposure time, which was intentionally varied in the range of +/-20% relative to the optimum.

The investigation revealed that:

use of the technique of screening for transfer of half-tone images makes it possible to employ standard photomasks with chromium coating;

the proposed method makes it possible to fabricate highly effective plane optical elements (kinoform lenses and aberration correctors) in photolithography equipment;

the photoscreening method has the greatest advantages for fabrication of elements with zone dimension less than 10-20 μm.

Bibliography

1. Koronkevich, V. P., Lenkova, G. A., Mikhaltsova, I. A., et al., "Kinoform optical elements: methods of design, fabrication techniques, practical application," AVTOMETRIYA, No 1, 1985

2. Koronkevich, V. P., Kirianov, V. P., Kokoulin, F. I., et al., "Fabrication of kinoform optical elements," OPTIK, Vol 67, No 3, 1984, p 257

3. Vedernikov, V. M., Vyukhin, V. N., Kiryanov, V. P., et al., "A precision photoplotter for synthesis of optical elements," AVTOMETRIYA, No 3, 1981

4. Vedernikov, V. M., Kiryanov, V. P., Korolkov, V. P., et al., "Lasernaya tekhnologiya izgotovleniya krugovykh shkal i kodovykh diskov [Laser technology for fabrication of circular scales and code disks]," Novosibirsk, 1986 (Preprint 319, Siberian department, USSR Academy of Sciences, IAiE)

5. Bryngdahl, O., "Computer-generated holograms as generalized optical components," OPT. ENG., Vol 14, No 5, 1975, p 426

6. Slyusarev, G. G., "Optical systems with phase layers," DAN SSSR, Vol 113, No 4, 1957

7. Koronkevich, V. P., Nagorni, V. N., Palchikova, I. G., Poleshchuk, A. G., "Bifocus microscope," OPTIK, Vol 78, No 2, 1988, p 64

8. U.S. Patent 4099829, "Flat field optical scanning system," R. J. Straayer, pub. 11 Jul 78

9. Brenden, B. B., Russell, J. T., "Optical playback apparatus focusing system for producing a prescribed energy distribution along an axial focal zone," APPL. OPT., Vol 23, No 19, 1984, p 3250

10. Bickel, G., Haeusler, G., Maul, M., "Triangulation with expanded range of depth," OPT. ENG., Vol 24, 1985, p 975

11. Kotletsov, B. N., "Mikroizobrazheniya: opticheskiye methody polucheniya i kontrolya [Microimages: optical methods of production and inspection]," Mashinostroyeniye, Leningrad, 1985

12. Lee Ming-Chin, Tseng Chau-Jern, Huang Chien-Rong, Huang Tzer-Hsiang, "A feasibility study on the use of amorphous silicon as optical recording medium," JAP. J. APPL. PHYS., Pt. 1, No 2, 1987, p 193

13. Poleshchuk, A. G., "The photoscreening method of kinoform synthesis for laser technology," "V Vsesoyuz. konf. "Optika lazerov" [The fifth all-union conference "Laser Optics"]," GOI im. Vavilova, Leningrad, 1986.

UDC 621.315.592:772.99

Kinoforms: Technologies, New Components and Optical Systems; Part II

907F0056B Novosibirsk AVTOMETRIYA No 4 Jul-Aug 89 pp 47-64

[Continuation of article under the "Optical Information Technologies" rubric by V. P. Korolkov, V. P. Koronkevich, I. A. Mikhaltsova, I. G. Palchikova, A. G. Poleshchuk, A. G. Sedukhin, A. P. Sokolov, Ye. G. Churin, and Yu. I. Yurlov, Novosibirsk]

[Text] **II. New Components.** For diffraction components, the difference in optical paths from the object to the image is not a continuous function of the coordinates at the pupil. In accordance with the generalized principle of tautochronism, it may be written as a+mλ, where a is a small portion of the wavelength λ, and m is any whole number. It can be taken that ordinary optical systems (m=0) are a particular case of diffraction systems. In this sense, diffraction components are often called generalized optical components [1, 2]. They can perform a more broad class of geometrical and wave transformations of images and fields than can the ordinary components.

The most simple and typical component is the diffraction lens. The topology of its zones coincides with the structure of Fresnel zones, while the complex transparency is equal to:

$$T(r) = \sum_{k=-\infty}^{\infty} c_k e^{-jkr^2/\lambda f}; \qquad (1)$$

$$c_k = \begin{cases} 0, & k \neq lN+1; \\ (-1)^l \dfrac{\sin\left[\pi\left(\frac{1}{N}+l\right)\right]}{\pi\left(\frac{1}{N}+l\right)} e^{-j\pi\left(\frac{1}{N}+l\right)}, & k = lN+1; \end{cases} \qquad l = 0, \pm 1, \pm 2 \ldots,$$

where f is the focal distance for the fundamental wavelength λ; r is the radial coordinate in the plane of the lens; N is the number of phase relief steps. When light passes through the lens, diffraction orders k=lN+1 arise, each of which corresponds to an addend of the sum (1). The proportion of luminous energy in the k-th order is equal to (the absolute value of c_k)^2 100%.

Let us consider three particular cases:

1. As N approaches infinity, the diffraction efficiency in the +1-st order approaches 100%. The phase profile of the lens corresponds to a profile with a "gleam." Such lens is commonly known as a kinoform. Its refraction counterpart is the planoconvex lens.

2. In the case N=2, we obtain a Rayleigh-Wood lens. The luminous energy behind the lens is mainly apportioned between the +1-st and -1-st orders. The diffraction efficiency in each of them is equal to around 40%.

3. When N=4, the diffraction efficiency of the +1-st order reaches 81%. This is the best possible case in practice, as the technological difficulties of fabrication are diminished, while the light losses are inconsiderable.

The boundaries of the circular zones of a diffraction lens are defined in accordance with the generalized principle of tautochronism: the difference between the optical paths of the rays passing through adjacent boundaries comprises a single wavelength λ. For the transformation of the parallel beam:

$$\begin{aligned} &\sqrt{r_m^2 + f^2} - f = m\lambda; \\ &r_m = \sqrt{2m\lambda f + (m\lambda)^2}, \end{aligned} \qquad m = 1, 2, 3, \ldots, M. \qquad (2)$$

Since the arrangement of the Fresnel zones coincides with the structure of the interference bands for lenses produced by holographic means, the diffraction lens is sometimes called a holographic or interference zone plate [3]. When $(m\lambda)^2$=0, the topology of the zones corresponds to a geometrical zone plate [4].

By changing the space frequency of the zones and their geometrical shape, a special kind of caustic may be formed, with or without conserving the projective properties of the system as a whole. A zone plate that concentrates radiation at a caustic with given lengthwise and transverse dimensions is known as a generalized plate. In this section, we shall present different versions of generalized zone plates, synthesized by a laser photoplotter.

The diffraction lens with increased focusing depth. Laser type image output systems and laser tangency measuring sensors operating by the triangulation technique [5] require components with enhanced depth of focus. The caustic of a diffraction lens may be changed in the necessary direction by introducing controllable aberrations, the problem being to maintain constant power of the flux of luminous energy along the focal segment in which the energy is concentrated.

Let us find the transmission function of the plate and relationships which connect the points of the focal segment with the radial coordinate. A refraction lens concentrates all of the luminous flux illuminating it at the focal spot. Through any given circular zone in the

plane of the exit pupil bounded by radii r and r+Δr there passes a flux of luminous energy of power:

$$\Delta W(r) \simeq 2\pi r \left|\frac{U(r)}{U(0)}\right|^2 \Delta r, \quad (3)$$

where U(r) is the amplitude of the illuminating wave in the plane of the lens. This power is concentrated in a region situated along the optical axis between points with coordinates z and z+Δz.

In the approximation of small angles of diffraction, the expression relating the phase transmission function Φ(r) and the focal distance z is valid:

$$d\Phi(r)/dr = -(r/z). \quad (4)$$

Combining (3) and (4) and requiring that the power be constant along the focal segment:

$$\Delta W(r)/\Delta z = 1/\xi, \ \xi - \text{const},$$

we obtain an equation for Φ(r):

$$\frac{d\Phi(r)}{dr} = -r\left\{2\pi\xi\int_0^r \left|\frac{U(r)}{U(0)}\right|^2 r\,dr + z_0\right\}^{-1}. \quad (5)$$

We shall assume that the illuminating wave is plane, homogeneous, monochromatic, and has unit amplitude. An analytical solution can also be found for a gaussian wave. In the approximation $\pi\xi r^2_{max}$ z_0 is much less than 1, equation (5) can be expanded in a Taylor's series, which enables the integration:

$$\Phi(r) = \Phi_0 - \frac{1}{z_0}\left\{\frac{r^2}{2} - \frac{\pi\xi r^4}{4z_0}\right\}. \quad (6)$$

The relationship between the points of the focal segment and the radial coordinate follows from expressions (4) and (6):

$$z(r) = z_0\left(1 + \frac{\pi\xi r^2}{z_0}\right). \quad (7)$$

With the help of (7), we determine the constant ξ:

$$r = 0, \ z = z_0,$$

$$r = R, \quad z = z_0 + \Delta z = z_0 + \pi\xi R^2 \rightarrow \xi = \frac{\Delta z}{\pi R^2},$$

where 2R is the light diameter of the zone plate.

Thus, the phase transmission function (6) has been obtained in the approximation $\Delta z/z_0 << 1$, which is tantamount to requiring a small depth of focus relative to the focal distance. Using the generalized principle of tautochronism, the radii of the zones are calculated from the condition:

$$z^2 + r^2_m = (z + m\lambda)^2. \quad (8)$$

Combining (7) and (8), we find:

$$r_m = \sqrt{2m\lambda z_0 + (m\lambda)^2}/(1 - 2m\lambda\Delta z/R^2),$$

which in the approximation $\Delta z/z_0 \ll 1$ дает

$$r_m = \sqrt{2m\lambda z_0 + (m\lambda)^2 + (m\lambda)^2 4z_0\Delta z/R^2 + (m\lambda)^3 2\Delta z/R^2}.$$

The first two terms of the radicand characterize the structure of the zones of an ordinary diffraction lens (see formula (2)). The third and fourth terms appear when Δz is nonzero in value. These introduce an extra, controllable aberration.

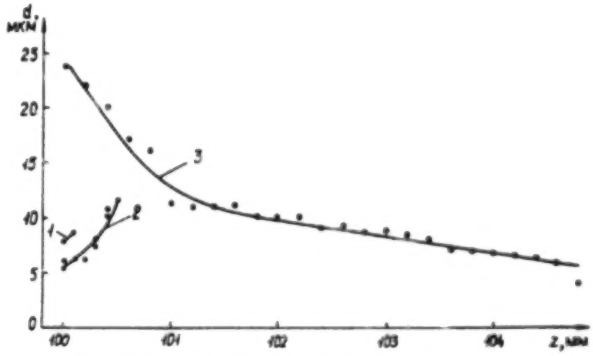

Figure 1. Experimental Relationship for the Change in Diameter d (μm) of the Focal Spot Along the Caustic: 1 - for a lens with focal distance z_0 =105 mm, 2 - for an aberrant lens (z_0=105 mm), 3 - for a generalized zone plate (z_0=100 mm).

A diffraction lens was synthesized with the following characteristics: focal distance z_0=5 mm, maximum radius R=10 mm, λ=0.63 x 10^{-3} mm. The results of an experimental investigation of its caustic are presented in Fig. 1 and 2. For comparison, similar measurements are given for an objective lens with focal distance of 105 mm and a lens with magnified spherical aberration (z_0=105 mm). Figure 1 shows the experimental curves of the change in diameter of the focal spot along the caustic. The elongation of the caustic for the zone plate, as compared to the traditional components, is clearly discernible. However, just as interesting is the distribution of the energy density along the axis of the caustic (see Fig. 2). Curves 1 and 2, corresponding to an objective lens and an aberrant lens, are shifted along the abscissa for convenience. The new component provides several intensity peaks, which are caused by interference of the stray diffraction orders. On the whole, the experiments are an excellent confirmation of the mathematical data.

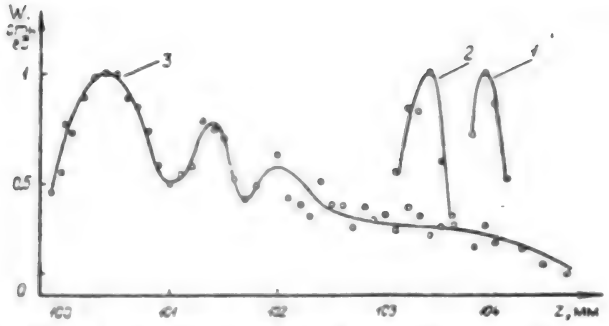

Figure 2. Experimental Curves of the Distribution of the Energy Density W (in Relative Units) Along the Axis of the Focal Segment: 1 - for an objective lens with focal distance z_0=105 mm, 2 - for an aberrant lens (z_0=105 mm), 3 - for a generalized zone plate (z_0=100 mm).

The logarithmic axicon. The phase transmission function of an axicon $\Phi_1(r)$, which provides constant intensity on the optical axis along the focal segment, is found by solving the differential equation of second order, obtained from the integral Kirchhof-Fresnel approximation by means of the stationary phase technique [6]. This has the form:

$$\Phi_1(r) = \tilde{\Phi}_1' \tilde{r} \ln(\tilde{r}^2 + r^2) + b. \qquad (9)$$

The parameters Φ'_1 and r are related to the wavelength λ, to the diameter of the beam waist d_0, and to its position on the optical axis z_0 by the following equations:

$$d_0 = 2{,}5\lambda/[\pi\tilde{\Phi}_1'(\tilde{r})]; \quad \tilde{r} = -\frac{\tilde{\Phi}_1'(\tilde{r})\, z_0}{\sqrt{1-\tilde{\Phi}_1'^2(\tilde{r})}}.$$

The constant b lets us shift the origin of coordinates, which is necessary to enumerate the zones. We find the radii of the zones of the axicon from (9):

$$\Phi_1(r_m) = m\lambda;$$

$$r_m = \sqrt{(\tilde{r}^2 + r_{\min}^2)\exp\left[\frac{\lambda m}{\tilde{\Phi}_1' \tilde{r}}\right] - \tilde{r}^2}.$$

In keeping with the calculation, an axicon was built, having the following parameters: light diameter 12 mm, length of focal segment 250 mm, diameter of spot at beam waist d_0=20 μm.

Results from measurement of the diameter of the light line are presented in Fig. 3 by the dots, the solid line corresponding to the calculation data. Figure 4 presents the results of an investigation of the distribution of the energy density along the focusing axis. The dots indicate experimental data from a single series of measurements. The straight line was constructed by processing the

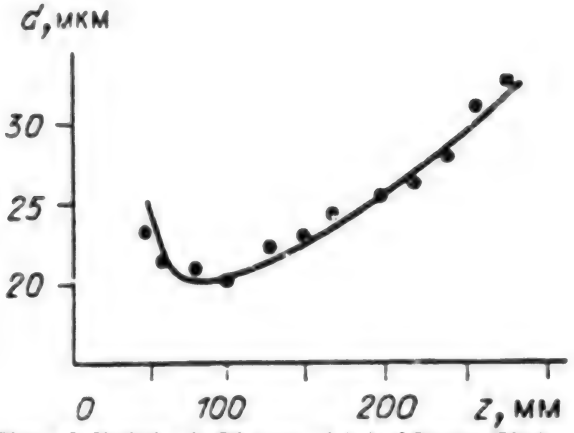

Figure 3. Variation in Diameter d (m) of Scatter Circle Along Focal Segment

measurement results of several series by the method of least squares. The calculated line is parallel to the abscissa, i. e., the axicon affords constant (within the limits of uncertainty) intensity on the axis.

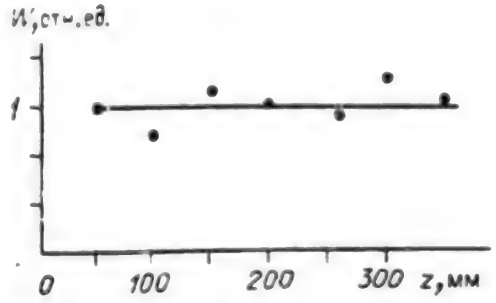

Figure 4. Distribution of Energy Density W (Relative Units) Along the Focusing Axis (z)

The axicon with lens. A new optical component was synthesized, combining the functions of a collimating objective lens and a glass cone. We call this component the lensacon. Its refraction counterpart is shown in the upper part of Fig. 5. Actually, the component integrates in space a Fresnel zone plate (lens) and a circular diffraction grating with constant interval (axicon).

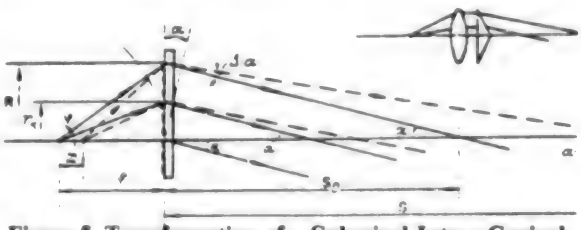

Figure 5. Transformation of a Spherical Into a Conical Wave With Constant Angle of Inclination of the Beams to the Axis α by the Lensacon

When the component is illuminated by a monochromatic pointlike source, situated at the front focus of the

lens, a luminous line is formed in the image space along the axis of the component. In the perpendicular plane, a nonlocalized Fresnel interference pattern is observed, namely, circular bands with a bright core at the center. The distribution of intensity in the interference field is described by the square of a zeroth order Bessel function of the radial coordinate [7].

The diameter of the first dark ring, bounding the central maximum, determines the diameter of the luminous line d. The radii of the diffraction zones can be calculated in the usual way, if we make the path difference of the rays traveling through the boundaries of the zones and the axial ray equal to an integer of the wavelength (see Fig. 5):

$$\sqrt{f^2 + r_m^2} - f + r_m \sin\alpha = m\lambda.$$

from this:

$$r_m = \frac{\sqrt{f^2 \sin^2\alpha + 2fm\lambda - m^2\lambda^2} - (f - m\lambda)\sin\alpha}{\cos^2\alpha}. \quad (10)$$

The terms are clearly evident from Fig. 5. The period of the lensacon zones does not remain constant, but diminishes from the center to the fringes. At the center, it is almost the same as $\lambda/\sin\alpha$. The period of the peripheral zones can be estimated as the period of the grating illuminated by the plane wave:

$$t \approx \lambda/[[r/\sqrt{f^2 + r^2}] + \sin\alpha]. \quad (11)$$

When the radiation source is placed exactly at the focus of the lensacon, the length of the luminous line is $S_0 = R/\alpha$; its diameter $d_0 = 0.766\lambda/\alpha$ does not depend on the distance L to the lensacon, since α is identical for all rays. In order to increase the length of the luminous line, it is necessary to bring the light source nearer to the component (see Fig. 5). Then:

$$S = \frac{R}{\alpha - \Delta\alpha} \approx R\Big/\left[\alpha - \frac{Rx\cos\varphi}{R^2 + f(f - x)}\right]. \quad (12)$$

In this case, the angle of intersection of the rays (shown in the figure by broken line) with the axis is not constant, but decreases from a value equal to α close to the lensacon, to a value R/S at the end of the line, and accordingly the initial and final diameters of the luminous line are equal to $0.766\lambda/\alpha$ and $0.766\lambda S/R$. Between these extreme values, d varies in linear manner, just as in the case of an axicon with constant period, illuminated by a spherical wave. It can be shown that the function d(L) has the form:

$$d(L) = 0{,}766\frac{\lambda}{\alpha}\left(1 - \frac{L}{S}\right) + 0{,}766\frac{\lambda L}{R}. \quad (13)$$

For practical purposes, we constructed amplitude lensacons having the following parameters: R=50 mm, f=300 mm, $\alpha = 10^{-2}$; R=25 mm, f=200 mm, $\alpha = 10^{-1}$; and R=20 mm, f=200 mm, $\alpha = 10^{-2}$. The first two components are intended to work with a helium- neon laser (λ=0.63 μm), the last with a semiconductor laser of the visible range (λ=0.63 μm). Investigation of these components revealed that the distribution of intensity in the cross section of the line may differ strongly from the square of the zeroth order Bessel function. Substantial distortions may be introduced into the luminous distribution by the nonplanarity and wedge shape of the substrates. The large wedge angle (as large as 1 angular minute) and nonplanarity of the surfaces in several of the bands produced astigmatism in the diffraction image, increasing with size of the zone radius. It was found that the nonparallelness of the surfaces for components with large diameter (2R around 100 mm) should not exceed 15 seconds. Errors of surface shape that are asymmetrical with respect to the center of a grating larger than $\lambda/20$ cannot be tolerated for any diameter of component. The precision of manufacture of the zone radii provided by the photoplotter (+/-0.25 μm) did not affect the quality of the image.

A photometric investigation of the distribution of intensity in the cross section of the line at various distances was performed for all the components. Several of the results are presented in Fig. 6.

The optical components, which combine in themselves the functions of a lens and a circular grating, have yet another advantage over the ordinary diffraction axicon [7]. High diffraction orders do not distort the distribution of intensity in the cross section of the line, since they are inclined toward the axis at a greater angle and lie outside the interference field after a distance of L=f.

Our component produces a substantial change in the caustic, increasing its lengthwise dimension, whereupon the projective properties of the optical system are not preserved. The specific applications for the new component are robot three-dimensional vision systems [5], inspection of straight alignment of machine tool bases, centering and installation of equipment.

Diffraction lenses for printers. The efficiency of recording of images in laser printers and technological systems with scanners depends on the distribution of energy over the cross section of the caustic and the constancy of the linear velocity of movement of the focal spot in the recording plane. In the case of a gaussian distribution, only a third of the energy is absorbed if the photoresponse of the medium has a threshold character. In order to form a specified energy distribution in the focal spot, recourse is had to zone plates, working in conjunction with modulating phase filters. Constancy of linear velocity during recording is achieved by the use of f lenses.

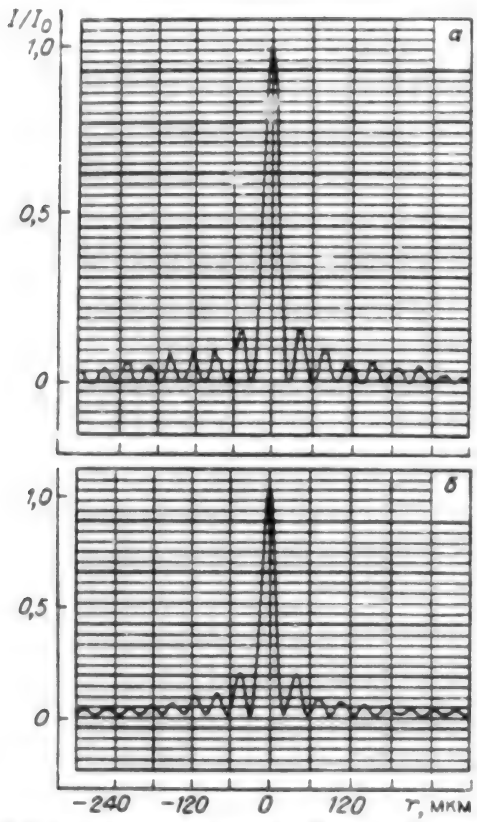

Figure 6. Distribution of Intensity in the Cross Section of the Luminous Line Formed by Lensacons With Parameters: a - f=300 mm, $\alpha=10^{-2}$, 2R=100 mm, λ=0.63 μm; b - f=200 mm, $\alpha=10^{-2}$, 2R=40 mm, λ=0.67 μm.

Key: 1. μm

1. MODULATED DIFFRACTION LENSES PRODUCING UNIFORM AND ANNULAR ENERGY DISTRIBUTIONS IN THE FOCAL SPOT [8]. Optimal utilization of the energy of the laser and improved efficiency of the recording process per individual component are achieved with a uniform distribution of the energy in the cross section of the caustic. In the continuous recording mode, an "annular" distribution is optimal. This problem is solved by means of a single optical component, which functions both as a diffraction lens and an axisymmetrical phase grating.

A simple and convenient method of calculating the transmission function of such component is to write it as the product of the transmission functions of the lens and a modulating phase filter.

The complex transparency function of the phase filter has the form:

$$T_1(r) = \begin{cases} 1, & R_1 < r < R; \\ e^{j\pi}, & r < R_1. \end{cases}$$

The distribution of the amplitude of the field in the focal plane is given by the convolution of the pulse response of the phase filter with the pulse response of the lens.

When the component is illuminated by a plane monochromatic wave, the distribution of intensity in the focal spot is found from the relation:

$$I(\rho) = \frac{4\pi P}{(\lambda f)^2}\left[\frac{J_1(\xi)}{\xi} - 2\left(\frac{R_1}{R}\right)^2 \frac{J_1(R_1\alpha/R)}{R_1\alpha/R}\right]^2,$$

where $\xi = 2\pi R\rho/\lambda f$; P is the full power of the radiation; ρ is the particular coordinate of the focal plane. By varying the parameter R_1/R (i. e., by varying the diameter of the entrance pupil), the distribution of energy in the spot can be controlled.

As the ration R_1/R increases, the radius of the focal spot grows and the distribution of the illuminance will have a quasirectangular form. Further increase in R_1/R will produce an annular distribution. The table presents the transmission functions of the phase filters (row 1), photographs of the focal spots (row 2), and experimental graphs of the scattering functions of the spot and the parameters of the components (row 3). For laser printers, an important characteristic of the focal spot is the power within a circle of chosen diameter. Results of such measurement are shown in the table. The use of diffraction components which combine in themselves the functions of a lens and a circular phase grating permits optimal coordination of the width of the line being recorded, the resolution and the power of the laser.

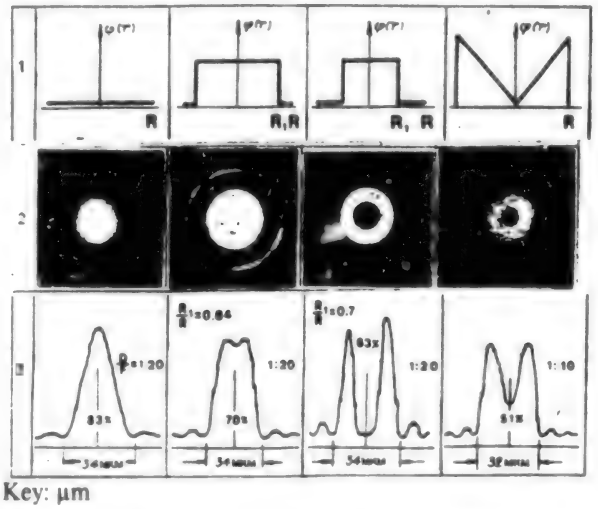

Key: μm

2. THE DIFFRACTION fθ LENS. The height of an image of an infinitely distant object in traditional lenses is proportional to f tg θ, where θ is the angle of incidence of the thin beam on the lens. In laser technological layouts and printers with large plane field, fθ lenses in

which the ordinate of the focal spot (height of image) is equal to fθ are needed in order to produce a constant speed of scanning.

The topology of the zones of a diffraction fθ lens is found by the beam path method, supplemented with the generalized tautochronism principle.

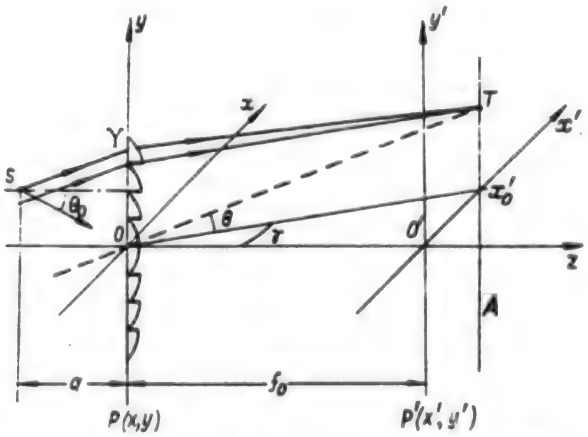

Figure 7. Geometry of Arrangement of an fθ-Zone Plate and the Scanning Line

Figure 7 shows the path of rays through the f lens for transmitted light. The scanning system (e g., a rotating polyhedron) causes the rotation of a narrow laser beam in the plane (z, y), such that the point S can be taken as the center of rotation. A zone plate is situated in the plane P(x, y). The focal spot moves in the scanning plane P' along line AT, parallel to the ordinate axis y'. The center of rotation S is displaced relative to the optical axis of the zone plate. The off-axis geometry makes it possible to remove the zeroth diffraction order from the scanning line. An arbitrary ray SY is deflected to (.)T, determined by means of the auxiliary ray OT, parallel to SY.

A zone plate which focuses a wide inclined beam to a point [9] has an elliptical zone structure, the boundaries of the steps of the kinoform relief being given by the equation:

$$(x - x_0')^2 + (y - F\Theta\cos\Theta)^2 + (F\cos\Theta\cos\gamma)^2 = (F - y\sin\Theta - \Delta\lambda)^2, \quad (14)$$

where

$$F = f/\cos\Theta_0\cos\gamma;\ \Delta = -((n/N) + m).$$

Let us write the canonical form of the equation (14) in the case of γ=0:

$$\frac{x^2}{A^2} + \frac{(y - y_0)^2}{B^2} = 1, \quad (15)$$

where

$$y_{0\Delta+1} = y_{0\Delta} - \lambda\,\mathrm{tg}\,\Theta/\cos\Theta; \quad (16)$$

$$A^2_{\Delta-1} = A^2_\Delta + \left[2F\left(\frac{1}{\cos\Theta} - \Theta\sin\Theta\right) + (2\Delta + 1)\lambda\right]\lambda/\cos^2\Theta; \quad (17)$$

$$B^2_{\Delta+1} = B^2_\Delta/\cos^2\Theta. \quad (18)$$

By specifying the number of relief steps N and the mask (step) number n and varying the number of the kinoform zone m from 1 to M, we may compute the set of parameters A, B, y_0 of the elliptical zone structure of a component which focuses a wide slanted beam into a point.

The problem of design of the fθ lens is more difficult because, in the first place, the angle of inclination of the illuminating beam θ is related to the y coordinate by the relationship y=a tg θ, and secondly, the beam has finite width. In actuality, this is a problem of linear programming: to find the solution of equation (14), describing certain curves on a plane and ensuring minimal aberrations on the beam width, subject to the additional condition y=a tg θ and the variable parameters N, m, n.

To solve this problem, the following method is proposed. Starting with the available information (slanting beams are focused by elliptical zone plates), we presume that the kinoform zones have the form of ellipses, and we perform the optimization of the parameters A, B, y_0 of each ellipse with numbers n, m, N in accordance with the requirement of minimizing the aberrations within the width of the illuminating beam.

Using equations (16)-(18), we calculate the next values of A, B, y_0 from the previous ones, introducing the necessary corrections for the angle of inclination of the beam θ. There are several ways of correcting ellipses. We shall consider two of them. Say the illuminating beam is quite narrow. The parameters of the first zone of the photomask are found from formula (14) with θ=0. Each subsequent (Δ+1) zone is computed from formulas (15)-(18), noting that the angle $\theta_{\Delta+1}$ depends on the quantity y_Δ as follows: $\mathrm{tg}\,\theta_{\Delta+1} = y_\Delta/a$.

The photomask consists of a set of elliptical zones, the centers of which are displaced as the number of zones increases. The pattern is symmetrical with respect to the x axis.

In this way, we can obtain an excellent approximation of the solution for beams whose width is on the order of several zones. It will be possible to improve the aberration properties of the diffraction fθ lens for wider beams if the correction of the parameters of the ellipses is done only until the Rayleigh condition is no longer met for the aberrations with respect to the central ray of the incident beam.

This discussion is easily extended to other versions of arrangement of the zone plate in the optical layout. Reflecting zone plates make it possible to circumvent power losses through absorption in the substrate, but

they have a large space frequency of the diffraction structure. The topology of the structure may be simplified by introducing an additional cylindrical lens.

The aspherical diffraction lens. The optical channels of the reading heads of optical memory devices make extensive use of lenses with one or two aspherical surfaces or hybrid components consisting of a refraction lens with kinoform corrector. We present below the calculation technique and the results of an experimental investigation of a diffraction lens which projects the body of emission of a semiconductor laser into the plane of a compact disk. A description of the reading head is presented in section III. Figure 8 shows the optical layout of the microlens of the reading head (the diffraction lens) and its parameters, found by the calculation.

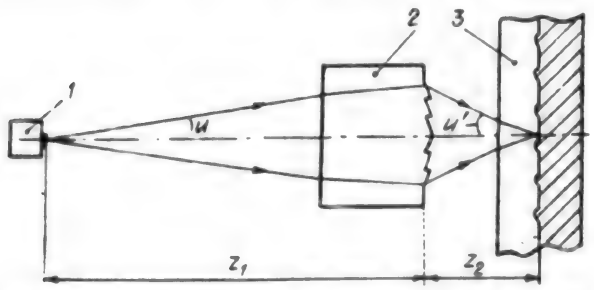

Figure 8. Optical Layout of the Microlens of a Reading Head:

Key: 1 - semiconductor laser (λ=0.79 μm), 2 - substrate with kinoform lens (thickness 3 mm, n=1.51), 3 - protective coating of disk (thickness 1.2 mm, n=1.49), sin u = 0.11, sin u' = 0.45, z_1 =11 mm, z_2=3.2 mm

It is assumed that the phase delay function of the element is even with respect to the radius, and therefore its derivative is approximated by the expression:

$$\frac{\partial \Phi}{\partial r} = \sum_{i=1}^{4} D_i r^{2i-1},$$

where r is the radial coordinate in the plane of location of the component; D_i are constant coefficients which are to be found.

For the phase delay function of the diffraction lens, the principle of superposition is met [10, 11], wherefore we can write: the partial derivative of Φ with respect to r in the form of the difference:

the partial derivative of Φ with respect to r = $n_2\beta(r) - n_1\alpha(r)$,

here α(r) is the directional cosine of the forward ray (from the source to the diffraction lens), and β(r) is that for the return ray (from the compact disk to the diffraction lens); n_1, n_2 are the indexes of refraction at the side of the forward and return ray, respectively.

The functions $n_1\alpha(r)$ and $n_2\beta(r)$ are approximated as follows:

$$n_1\alpha(r) = \sum_{i=1}^{4} A_i r^{2i-1}, \quad n_2\beta(r) = \sum_{i=1}^{4} B_i r^{2i-1}.$$

In order to find the coefficients A_i and B_i, we use a standard program for design of axisymmetrical refraction optical systems in computer, by means of which the values of the directional cosines in the forward and the return path of the rays are calculated at four points on the surface of the diffraction component; it is not at all necessary that these points coincide, as is presumed in [12], for example, since the choice of points for the interpolation of a smooth function has rather great latitude.

After this, we solve two systems of four linear equations:

$$\sum_{i=1}^{4} A_i r_k^{2i-1} = \alpha(r_k)\, n_1 \quad (k = 1, 2, 3, 4);$$

$$\sum_{i=1}^{4} B_i r_j^{2i-1} = \beta(r_j)\, n_2 \quad (j = 1, 2, 3, 4),$$

where r_k and r_j are the coordinates of the points for which the directional cosines of the forward and return rays have been calculated. Introducing the definition $D_i=B_i-A_i$ we find:

$$\Phi(r) = \int \frac{\partial \Phi}{\partial r}\, dr = \sum_{i=1}^{4} \frac{D_i}{2i} r^{2i} + \Phi_0,$$

where Φ_0 is an arbitrary constant, not affecting the functioning of the diffraction lens. It is convenient to vary the value of this constant when calculating the radii of the kinoform zones by the formula $\Phi(r_m)=m\lambda$.

The accuracy of evaluation of the function Φ(r) for a light diameter of 2.8 mm, an aperture angle of 0.11 in the object space and 0.45 in the image space was λ/32 (λ=0.79 μm).

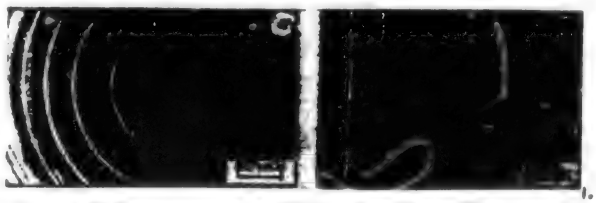

Figure 9. Fragments of a Diffraction Lens Obtained in the Scanning Microscope

Key: 1. μm

The photomask of the diffraction lens was made by the thermochemical technique [13] with tenfold magnification. Next, using the UER step- and-repeat camera, the image of the lens was reduced and multiplied on standard glass plates for photolithography, 102x102x2.5 mm in size. Etching of the glass through a mask (chromium or iron oxide) was done in an ionic radiation etching layout, using argon or carbon tetrafluoride. The masking coating was then removed. Figure 9 shows the resulting images of the diffraction lens, taken in scanning electron microscope: the central region (a) and the zones at the edge of the lens (b). The minimum width of the zones was 0.61 μm, the depth was around 0.8 μm. Photographs of the scatter circles of the diffraction lens (a) and, for comparison, a series produced lens (b) of the KSS-123 head from Sony, taken at identical magnification, are shown in Fig. 10. The diameter of the spot is 2.1 μm, the diffraction efficiency of the lenses made with binary profile is 25-30%.

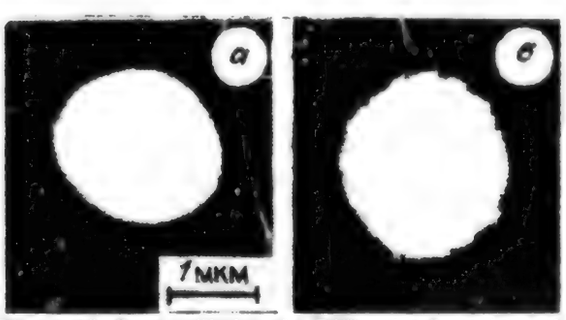

Figure 10. Scatter Circles of a Diffraction Lens (a) and the Series Produced Lens of the Sony KSS-123 Head (b)

Screens with diffraction lines (gradations). An important advantage of the laser photoplotter is its ability to synthesize radial gratings, precision circular scales, code dials, and master optical memory disks. Let us consider a radically new optical component—gratings with diffraction lines. These components have been investigated in detail in [14, 15]. In diffraction gratings, as opposed to conventional gratings (Fig. 11, a), there is an additional screening of lines in the direction perpendicular to the direction of their alternation (Fig. 11, b). In the double screening, the light-modulating lines of conventional scales are replaced by light-deflecting lines, produced as unidimensional diffraction gratings or zone plates. In contrast with standard ruled scales, we are able to synthesize components whose lines possess focusing ability and make it possible to organize optical cross connections during data encoding. This allows an increase in the volume of information transmitted, since each line is now able to deflect light at different angles.

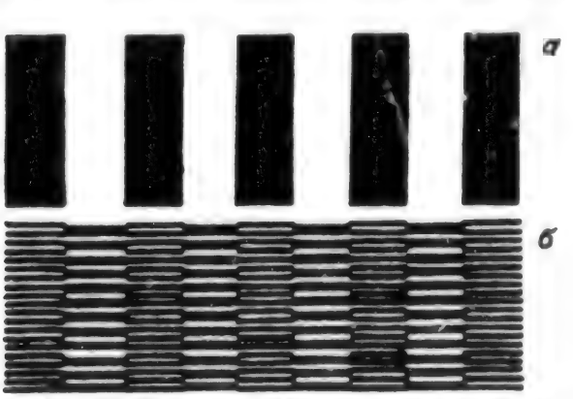

Figure 11. Comparison of Structures of an Ordinary Unidimensional Screen (a) and a Screen With Diffraction Lines (b)

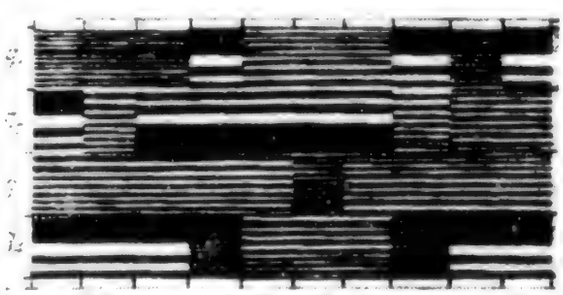

Figure 12. Fragment of a Simplified Structure of a Code Scale Based on a Screen With Diffraction Lines

Figure 12 shows a simplified picture of a fragment of the scale of a diffraction code screen. The scale is deposited on the peripheral portion of the disk and consists of four code tracks q_1, ..., q_4. The individual gradations of each track consist of elements of kinoform lenses. Thus, for example, the first sectors of the tracks q_1 and q_4 belong to one lens, while those of tracks q_2 and q_3 belong to another, and the optical centers of these lenses are displaced relative to each other, so that the light focusing occurs at spatially separated points, associated with different photoelements of the information reading system. As the code scale is shifted, the light will be redistributed among the sectors of the line of photoreceivers, i. e., such scale acts as a multifocus diffraction lens, having one or more light focusing regions in accordance with the code combination.

Unlike the standard ruled scales, diffraction scales have a larger information capacity, and also allow better accuracy of reading the position of the dial and better noise immunity in the information encoding, thanks to checking (for example) that the sum of signals registered from all code tracks is constant. When the gratings are working in reflected, linearly polarized light, it is possible to devise an information reading layout such that the process is moved into the region of anomalous Wood diffraction [16], thereby greatly enhancing the diffraction efficiency of the component.

III. **Optical systems with kinoform components.** The use of diffraction components makes it possible to reduce the number of components in optical systems, thanks to

unification of the functional properties of several components in a single one. Kinoforms, in conjunction with ordinary optical components, make it possible to reduce the overall size, weight, and cost of traditional optical devices and create fundamentally novel and unprecedented optical systems.

The old masters corrected the quality of optical systems by "retouching:" with fine polishing down to fractions of a wavelength, they would apply artificial defects (local and zonal) to the surface of the lens, which lessened the wave aberration of the system as a whole. Actually, this process made intuitive use of the fundamental principles that underlie the functioning of modern day optical systems, consisting of refraction and diffraction components.

We present below the results of an experimental investigation of various optical systems, consisting of classical and kinoform components.

The bifocus microscope. Coincidence microscopes are used for observation of micro-objects (brands, crosshairs, coincidence marks) located in different object planes and for placing them on a single line. In typical contact photolithography applications, the distance between the object planes is usually 5-20 μm. In X-ray lithography coincidence layouts using synchrotron radiation, the distance between the substrate and the X-ray mask reaches 20-100 μm, and a microscope with enhanced depth of definition is required to observe them at the same time.

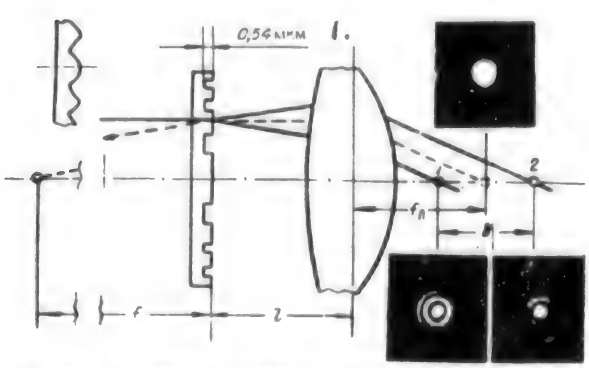

Figure 13. Optical Layout of a Bifocus System in the Return Path of the Rays

Key: 1. 0.5μm

In the present work, we give the results of an investigation of a bifocus microscope [17], the optical layout of which includes diffraction elements: a Rayleigh-Wood lens or zone plate with special phase profile of the zones, shown in the upper left portion of Fig. 13. Also shown here is the optical diagram of the bifocus system in the return path of the rays. The Rayleigh-Wood lens behaves like a combination of scattering and collecting lenses at the same time. A parallel pencil of rays impinging on the diffraction lens is divided such that 81% of the energy is distributed equally between the foci of +1-st and -1-st order. The rays diffracted in the +1-st order are collected in front of the focal plane of the lens at point 1; those diffracted in the -1-st order are focused at point 2. The distance between the points 1 and 2 (when f is much greater than f_n and f is much greater than l) can be found from the simple relation:

$$\delta \simeq 2f_n^2\lambda_0/\lambda_0 f.$$

Here, λ_0 is the wavelength for which the Rayleigh-Wood lens has been designed; λ is the working wavelength. The other terms are clear from Fig. 13. When f_n=10 mm, f=1000 mm, l=0, the distance between the micro-objects δ varies from 150 to 200 μm in the spectral range of 656-486 nm. To eliminate chromatic aberrations, it is necessary to limit the width of the spectrum of the light source to $\Delta\lambda=(\lambda/D)^2 f$. When $\lambda=0.55\times10^{-3}$ mm, D=4 mm, f=1000 mm, the permitted spectral range is $\Delta\lambda$ around 5 nm, which makes it possible to use ordinary light sources with interference light filters. A substantial defect of this bifocus system is the scattered light caused by the presence of diffraction orders above the first. This may be remedied by using a special kinoform lens in the form of a circular zone plate. The phase relief within the even-numbered zones corresponds to that of a collecting lens, that inside the odd-numbered a scattering lens, varying from 0 to 2π according to a quadratic law (see Fig. 13). In order to minimize wave aberrations, it is necessary to use lenses with the maximum possible focal distance and arrange the objects being observed in the focal planes of the bifocus system.

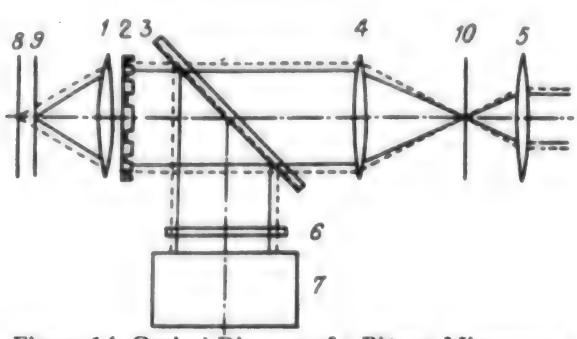

Figure 14. Optical Diagram of a Bifocus Microscope Working in Reflected Light

Figure 14 shows one of the versions of the optical diagram of a bifocus microscope working in reflected light. The microscope illuminator 7 is designed in a Keller layout and ensures a telecentric path of the rays through the microlens 1 with kinoform adapter 2. A Rayleigh-Wood lens is located in the exit pupil of the microlens, forming with it a bifocus system. Such arrangement ensures optimal illumination of both object planes. The rays of light reflected from the substrate 8 and the photomask 9 return through the bifocus system, move through a light- dividing plate 3, and land on the

barrel lens 4, which aligns the images of the micro-objects in the plane 10. The image is viewed in the eyepiece 5. An interference filter 6 is used to isolate a narrow spectral band. Adjustment of the transmission band can be done by shifting or tilting it relative to the optical axis. The linear magnification of the system of microlens, kinoform lens, and barrel lens is found in the usual manner for each object plane.

An experimental verification of the proposed system was performed with microlenses 16/0.2 and 6.3/0.65. A Rayleigh-Wood lens of 8 mm diameter (f=1000 mm, λ_0=0.55 μm) was made by the photolithography technique, using reactive ionic etching. The distribution of light near each of the foci has the characteristic form for a small primary spherical aberration. The radius of the first dark ring of the diffraction spot is 1.9 μm for the microlens without adapter; for the bifocus system, the first focus is 1.85 μm, the second 1.87 μm. A mathematical simulation of the process of distortion of the light distribution near the focus with spherical aberration present was performed. The nature of the distortions is entirely determined by the amount of the wave aberration. Comparison of the calculated curves with experimental ones makes it possible to find the order of magnitude of the spherical aberration of the system, which is around 0.9λ for each of the foci. The distribution of luminous energy between the foci is 43.1% for the first focus and 49.3% for the second.

The results obtained and the expert evaluations that were performed allow the conclusion that it is possible to use microlenses with kinoform adapter in standard coincidence microscopes to impart bifocal properties to them. The example presented shows that kinoforms can be used to control the distribution of energy at the caustic while preserving the projective properties of the optical system.

The laser slide wire. To check for straightness of the guideways of large machine tools and line up equipment on a straight line, an instrument was built in which the element forming the luminous sighting line is a lensacon. Figure 15 shows the optical schematic of the laser slide wire. The emission of a helium-neon laser 1 is focused by a microlens 2 at a point situated close to the focus of the lensacon 3. Behind the element is a matrix photoreceiver 4, coupled with the base of the machine being inspected; 5 is a recording device. The mission is to determine the displacement of the photoreceiver relative to the optical line produced by the source and the center of the lensacon.

For practical purposes, it was necessary that the length of the optical line be 50 m, and its cross section not exceed 500 μm. It is clear from expression (13) that this condition is met when the linear aperture of the element 2R is equal to 100 mm. It is necessary to satisfy two requirements in selecting the focal distance: 1) reduce the overall size of the instrument; 2) enable a good quality

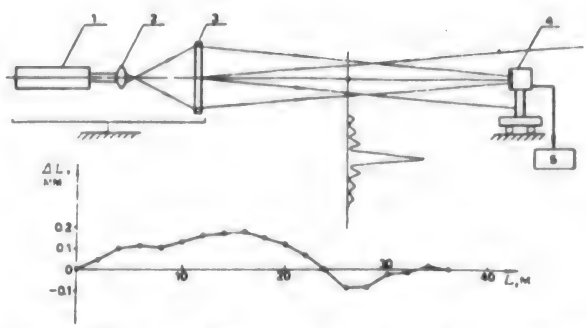

Figure 15. Optical Schematic of the Laser Slide Wire

photolithographic copying, for which the width of the zones should be greater than 1.5 μm. A focal distance of 300 mm is optimal.

Lensacons with light diameter of 100 mm, f=300 mm, and $\alpha=10^{-2}$ were made on high quality substrates. When illuminated by a point source with λ=0.63 μm, located at the focus, the elements form a luminous line of length 5 m with constant diameter of the central bright spot of around 50 μm. By moving the source toward the lensacon, we obtain a line of varying length, from 5 to 50 m. Investigations of the elements were performed with the length adjusted to 5 and 25 m. The straightness of the line was verified by the standard technique [18] with repeated back and forth movement of the guideways and the lensacon in two positions relative to the axis: 0 and 180°, which excluded the influence of nonstraightness of the guideways. The deviations from straightness of the luminous line of the lensacon did not exceed 15 μm.

The lower part of Figure 15 shows the results of an inspection of a machine base of length 36 m under factory conditions. The mean quadratic error did not exceed 40 μm.

We should point out that the laser slide wire is a very simple device, actually consisting of only one optical element, the lensacon, since the microlens shown in Fig. 15 can be eliminated by using a semiconductor laser, the emission body of which is a pointlike source.

The read head for a laser disk player. In digital laser players, the playback of the information recorded on the disk is done by a read head, the optical channel of which is a complex projection system. This system transfers the body of emission of a semiconductor laser into the plane of the compact disk and back through a light divider to the photoreceiving matrix. In addition, the optical layout of the head includes sensors for automatic focusing and tracking.

The most sophisticated read heads of the world's leading companies (Philips, Sony, Matsushita, etc.) employ a technology of manufacture of high quality aspherical lenses by casting from glass or plastic. This has made it possible to create heads consisting of no more than 5 to 7 components. Further progress involved the use of integrated and diffraction optics, so that all the main

assemblies could be produced by the well known photolithography process of the electronics industry. The recourse to diffraction optics necessitated a revision of the optical layout design philosophy. In the system which we proposed [19], the disk illumination and information reading channels were spatially separated. It is clear from Fig. 16a that the head consists of no more than two components: a semiconductor laser 1 and an optical module 2 with photoreceivers 5, 6.

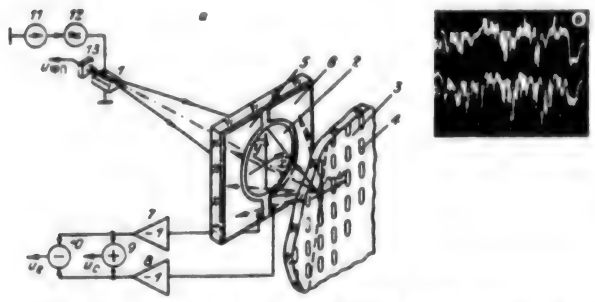

Figure 16. Layout of the Read Head With Diffraction Focusing Lens and Annular Photoreceiver (a) and Oscillograms of the Voltage at the Outputs of the Summer and Subtractor (b)

Such head in its specifications (dimensions, weight, etc.) is not inferior to the head [20], made in the form of an integrated optical circuit. The reading photoreceivers 5, 6 have an annular shape and are mounted coaxially with a diffraction lens 2 (they can be made on a single substrate of glass or sapphire). The separation of the annular photoreceiver into individual sectors (two or four) ensures the formation of the electric signals needed for the operation of the tracking and automatic focusing systems.

The head works as follows. The optical emission of a semiconductor laser 1 is focused by the diffraction lens 2 onto the surface of the compact disk 3. If no information "pits" 4 are present, the light is reflected from the surface of the disk as a mirror, returns through the lens, and is sent back to the laser. When the reading spot lines up with a "pit," the luminous flux is diffracted by it and scattered in a considerable solid angle. The diffracted flux (broken lines) is perceived by the annular photoreceiver, whose sectors 5, 6 are connected via matching amplifiers 7, 8 to a summer 9 and subtractor 10. These latter put out an information signal and a tracking signal, respectively. If no "pits" are present, the luminous flux hardly reaches the photoreceiver and therefore the depth of modulation of the information signal approaches 100%, which makes it possible to reproduce the digital information with a high level of accuracy.

A distinctive feature of this layout is the appearance of optical feedback, caused by the light reflected from the surface of the disk 3 reaching the laser cavity 1. The optical feedback results in increased level of noise of the laser emission. To eliminate this, we introduced (via assembly 12) a modulation of the power supply current of the laser with frequency of 50-100 MHz. This does not allow the random mode skipping that results from the optical feedback. The modulation of the current of the laser and, thus, the emission frequency does not influence the process of information reading, since the modulation frequency is much higher than that of the information signal.

The optical emission from the other end of the laser 1 is received by a built-in photoreceiver 13, the output signal of which is used for the operation of an emission power stabilization system 11.

The experimental model built after the diagram in Fig. 16a employed the ILPN-210 single-mode semiconductor laser and a diffraction lens of 2.8 mm diameter. The design of the structure of the aspherical lens and the results of its testing have been presented in the previous section. Two nonencapsulated silicon photodiodes of dimension 2.5x2 mm were glued directly to the glass backing of the diffraction lens. The compact disk, placed in the focal plane of the lens, was moved by a servo element such that the reading spot of the head intersected the information tracks at an angle of approximately 2° (in Fig. 16a, the trajectory of motion in the disk plane is shown by broken line). Figure 16b shows oscillograms of the sum 1 and difference 2 of the output signals of the photodiodes. The appearance of voltage pulses on the outputs of the photodiodes corresponds to the moments of intersection of the reading spot and the information "pits." It follows from the oscillogram that, when the centers of the reading spot and the information track coincide, the amplitude of the sum signal reaches its magnitude, while the polarity of the difference signal is reversed. The sum signal can be used to operate the decoder of a player, while the difference signal (after averaging) can be used to operate the radial tracking system.

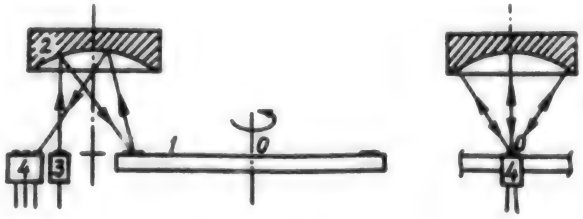

Figure 17. Optical Diagram of an Angle-Code Converter

The angle-code converter. Figure 17 shows the optical layout for reading of information from a circular dial 1, the scale rulings of which are made in the form of unidimensional diffraction gratings. The center of rotation of the dial is designated by 0. The reading head consists of a spherical retroreflector 2, a light source 3 (semiconductor laser), and a line of photoreceivers 4. The light from the source 3 after the first reflection by the retroreflector 2 lands on the scale rulings of the dial 1. Each ruling is a diffraction grating in the form of a

Fresnel zone plate. The scale actually consists of a collection of narrow reflecting diffraction lenses with different displacement of the optical centers and allowing the light after a second reflection from the retroreflector 2 to be collected on the line of photoreceivers 4. The angles of incidence of the light on the scale of the dial and the angles of diffraction are chosen such that each grating operates in the region of the Wood anomaly. As the dial is turned, the next scale ruling (whose grating has a different displacement of the optical center) moves into the illuminated reading zone. After diffraction reflection from the new ruling, the beam of light will move to the next area on the line of photoreceivers 4.

Figure 18 [not reproduced] shows a magnified fragment of the structure of the dial scale. At the center of the fragment can be seen the spatial gap between adjacent rulings. The scale was synthesized in a laser photoplotter and has a mean zone period of 0.9 μm. Figure 19 [not reproduced] shows the patterns of distribution of illuminance on the line of photoreceivers when the first type of ruling, the spatial gap between adjacent rulings, and the second type of ruling are located in the reading zone.

Conclusion. The above results illustrate the capabilities of laser computer phototechnology. The design of the optical component and its fabrication are practically combined into a single technological cycle. The combination of the professions of optical designer and fabricator substantially alters the situation and will encourage the appearance of new components for which classical optics has no counterparts. For the first time, the optician will master the skill of fabricating a precise optical surface of arbitrary shape and become able to create components with given energy distribution in the caustic.

The advent of the new components will encourage the development of optical instruments and arrangements distinguished by simplicity of design and enabling mass duplication without substantial material expenses.

Bibliography

1. Bryngdahl, O., "Computer-Generated Holograms as Generalized Optical Components," OPT. ENG., Vol 14, No 5, 1975, p 426

2. Slyusarev, G. G., "Optical Systems With Phase Layers," DAN SSSR, Vol 113, No 4, 1957

3. Young, M., "Zone Plates and Their Aberrations," JOSA, Vol 62, No 8, 1972, p 972

4. One, Y., Nishida, N., "Holographic Laser Scanning Using Generated Zone Plates," JOSA, Vol 21, No 24, 1982, p 4542

5. Bickel, G., Haeusler, G., Maul, M., "Triangulation With Expanded Range of Depth," OPT. ENG., Vol 24, 1985, p 975

6. Palchikova, I. G., "Sintez fazovoy struktury kinoformnykh aksikonov [Synthesis of the phase structure of kinoform axicons]," Preprint 328, Siberian division, USSR Academy of Sciences, IAiE, Novosibirsk, 1986

7. Mikhaltsova, I. A., Nalivaiko, V. I., Soldatenkov, L. S., "Kinoform optics," OPTIK., Vol 67, No 3, 1984, p 267

8. Palchikova, I. G., Poleshchuk, A. G., "Kinoforms for laser information recording systems," "Tez. dokl. V Vsesoyuz. konf. "Optika lazerov" [Abstracts of reports of the Fifth All-Union Laser Optics Conference]," GOI, Leningrad, 1986

9. Lenkova, G. A., "A Rotating Focusing Kinoform," AVTOMETRIYA, No 6, 1985

10. Gan, M. A., "Computer Modeling of Holographic Correction of Aberrations of Optical Systems," OPTIKA I SPEKTROSKOPIYA, Vol 41, No 4, 1976

11. Bobrov, S. G., Greysukh, G. I., Turkevich, Yu. G., "Optika difraktsionnykh elementov i sistem [Optics of diffraction components and systems]," Mashinostroyeniye, Leningrad, 1986

12. Paritskaya, G. G., Medvedev, V. S., "Design of the Path of Rays Through Optical Systems Containing GDR," OMP, No 3, 1975

13. Vedernikov, V. M., Kiryanov, V. P., Korolkov, V. P., et al., "Lazernaya tekhnologiya izgotovleniya krugovykh shkal i kodovykh diskov [Laser technology of fabrication of circular scales and code disks]," Preprint 319, Siberian division, USSR Academy of Sciences, IAiE, Novosibirsk, 1986

14. Sedukhin, A. G., "Preobrazovateli informatsii na osnove rastrov s difraktsionnymi gradatsiyami [Information converters based on screens with diffraction gradations]," Preprint 359, Siberian division, USSR Academy of Sciences, IAiE, Novosibirsk, 1987

15. USSR patent 1292181, "A Displacement To Code Converter," A. G. Sedukhin, published 23 Feb 1987, BYUL. No 7

16. "Electromagnetic theory of gratings," ed. by R. Petit, Springer Verlag, Berlin, Heidelberg, New York, 1980

17. Koronkevitch, V. P., Nagorni, V. N., Palchikova, I. G., Poleshchuk, A. G., "Bifocus microscope," OPTIK, Vol 78, No 2, 1988, p 64

18. Yambayev, Kh. K., "Vysokotochnyye stvornyye izmereniya [High precision range measurements]," Nedra, Moscow, 1978

19. Koronkevich, V. P., Poleshchuk, A. G., Palchikova, I. G., "Information reading from compact disks by a laser head with diffraction optics," KVANTOVAYA ELEKTRON., No 10, 1988

20. Osamu, W., et al., "Recent progress in optoelectronic integrated circuits," IEEE QUAN. ELECTRON., QE-22, No 6, 1986, p 805

Optimization of the Power Reserve when Planning the Expansion of Energy Systems with Allowance for the Implementation of Scheduled Repairs

907F0100A Kishinev IZVESTIYA AKADEMII NAUK MOLDAVSKOY SSR: SERIYA FIZIKO-TEKHNICHESKIKH I MATEMATICHESKIKH NAUK in Russian May-Aug 89 pp 51-56

[Article by F. D. Goldenberg, P. A. Malkin, and T. N. Pluzhnikova]

[Text] One of the most crucial problems to be solved in the planning of the expansion of the Unified Electric Power System (YeES SSSR) and the unified power systems of the country is the analysis of the reliability and the calculation of the power reserve. The overall required power reserve in future is found as the sum of two kinds of reserve—the repair and the operating [1].

The repair reserve is provided to make it possible to carry out scheduled repair jobs on the primary equipment of the power stations and it includes the following components: the reserve for carrying out current maintenance, the reserve for carrying out major overhaul, and an extra reserve for carrying out expanded rehabilitation repair (modernization) of power station equipment that has outlived its specified operating term.

The operating reserve is designed to balance out an emergency drop in power generated by the system as a result of failures in the equipment of the power stations and the main electricity transmission lines, and also to balance out random and unforeseen deviations in the available power of the stations (including the startup of newly introduced units), or a load in excess of the scheduled levels.

The optimum is a minimal power reserve, enabling the requisite reliability, which is defined as the probability of an operation with no shortages.

Scheduled major and intermediate repair of equipment is done, whenever possible, during the time of the seasonal load decrease, in the so- called trough of the annual load chart. If there are no constraints in terms of operating duty or repair process, then in the event that the area of the trough is larger than the required volume of major and intermediate repairs (the sum of the products of the power of the units put into scheduled repair and the duration of the repair), no reserve is provided to perform the major and intermediate repair.

Owing to the substantial increase in the share of large units of atomic and thermal power stations in the future structure of the generating facilities, the increase in the repair area in the European portion of the YeES SSSR will exceed the increase in area of the trough of the load chart, and therefore at a certain stage of its expansion it will be necessary to have a reserve in order to carry out the major overhaul. The size of the required reserve will depend on the implementation of the repairs, i. e., the chosen principle of designating the configuration of the repair area. Several aspects in the investigation of this relationship are presented in the current article.

As the tools of the investigation, we employed the procedure and the program package "Sostav," worked out by the department of power industry cybernetics of the Moldavian SSR Academy of Sciences [2].

The program package is designed to evaluate the reliability and determine the complements of working, reserve, and repaired units in each formal interval of the year on the basis of an optimal distribution of the operating and repair power reserves during the solving of the problem of planning the expansion of the power systems.

The criterion of optimality in the distribution of the power reserves is a minimum mathematical expectation of the annual shortfall in production of electricity.

The "Sostav" package has two basic operating modes, each of which defines a different degree of accuracy and computer costs when calculating the required reserves and evaluating the reliability: approximate "Proyektnyy," where the planned repairs are factored in as repair areas, while the change in the equipment complement during the year is factored in as the so-called load conditions; and the more precise "Ekspluatatsionnyy," in which an optimal chart of the annual planned repairs is constructed, and the change in equipment complement during the course of the year is considered in the reliability assessment.

The following initial information is used in the calculations:

—data on the generating equipment of the stations: the installed and the available powers of the unit, the seasonal drops and underutilization of capacity, the type of fuel, the time for installation or disassembly, the duration of the modernization;

—the coefficients of the monthly load maxima (adjusted to their absolute overall maximum);

—the coefficients of the characteristic daily load charts (adjusted to the monthly maximum), indicating the serial number of the first and last week of the respective characteristic season of the year;

—the standard deviation of the load from the annual maximum on account of error in prediction and irregular fluctuations in the maximum;

—the load maxima (proper load and composite load) and the consumption of electric power by the particular power system (including power transfers);

—the failure rates, the normative periodicities and durations of major, intermediate, and current repairs according to type of unit;

—the minimum permissible interval between two scheduled repairs of units performed during the same year;

—the maximum permissible number of units placed in scheduled repair at the same time, according to each type;

—the maximum capacity of units undergoing simultaneous repairs, and so forth.

The calculations are done with respect to a unified power system, characterized by the following parameters:

—load maximum 61.5 GW;

—area of trough in annual load chart 204,300 MW-weeks;

—structure of the units: atomic 40%, combination 33%, thermal 16%, hydraulic 11%;

—repair area, determined by mean annual norms of major repairs, 415,600 MW-weeks.

The relationship between the repair area and the area of the trough shows that an extra reserve is needed in the power system to implement the planned repairs. Optimization of the operating reserve by redistribution of repairs within the year involves construction of such equipment repair chart as ensures:

—maximum reliability for the given available capacity of the power system;

—minimum required generating capacity, i. e., minimum overall reserve, for a given reliability level.

If the assessment of the reliability does not consider the change in complement of working units as a result of placing them into planned repair, the optimal repair strategy ensuring maximum reliability will entail balancing out the operating reserve as much as possible over all intervals within the year. In particular, in the event that the required repair area is greater than the area of the annual load drop, the operating reserve for an optimal repair schedule will be constant over the course of the year. With such approach, the nominal required reserve for this power system will be equal to 23.4%, including an operating reserve of 14.2%, a repair reserve of 9.2%, and (within the latter) a reserve for major overhaul of 1.8%. The ratio of imbalance in the repair process (overhaul and modernization), defined as the ratio between the maximum and the average capacity of equipment placed in repair, is 1.78. In actual fact, the change in complement of working units as a result of placing some of them in repair results in a lower probability of emergency power drops. Since the planned repairs during the summer period reach 20-25% of the equipment capacity, and this the largest equipment, the outcome of this change is substantial. As a result, an equal reliability during the summer period may be achieved with a lesser value of the operating reserve than that in the winter. Hence, it becomes possible to increase the summer repairs even further, with a corresponding diminution in the winter repairs and, thus, a reduced requirement for reserve capacity. The optimal strategy for carrying out scheduled repairs roughly corresponds to equality of the relative values of the operating reserve during the intervals, i. e., equal ratios between operating reserve and load of the interval.

For a given available capacity, the distribution of repairs with allowance for the change in equipment complement is equivalent to an increase in the operating reserve by the approximate ratio of P/P_m, which thus corresponds to an increase in reliability.

Here, P is the mean annual load, averaged over the monthly maxima, and P_m is the load of the maximum month. When searching for the optimal reserve, the specified reliability is achieved at lower available capacity.

In our example, optimal distribution of the repair jobs made it possible to reduce the required power reserve from 23.4 to 21.7%, the operating reserve during the maximum period being 13.8% and during the minimum 11.2% (Fig. 1a). In Fig. 1, the solid lines N_{pac} and N_{pem} indicate, respectively, the available capacity of the system and the upper limit of the repair area, found from the condition of equality of the operating reserve during the course of the year. The broken line shows the upper limit of the optimal repair area N_{pem} in terms of reliability and the corresponding levels of the available capacity N_{pac}.

Of course, optimization of the scheduled repair jobs makes their implementation less uniform throughout the year, so that the imbalance factor increased from 1.78 to 1.92.

If the power system is operating within an amalgamation, a fundamental opportunity for combination of repair jobs is created.

Say, for example, that two power systems are amalgamated, one of which has a shortage in repair area due to a preponderance of atomic and thermal power stations, while the other has a surplus. In the system with a shortage it is then possible to further redistribute the repair jobs (broken line N_{pem} in Fig. 1b), increasing them in the summer months by lowering the operating reserve, under the expectation that emergency situations will be handled by a transfer from the system with a surplus. The decrease in repair jobs during the winter period, achieved in this way, increases the reliability or makes it possible to decrease the necessary repair reserve. In our example, total elimination of winter major overhaul is achieved with an external power transfer of as much as 3000 MW, while the required overall power reserve may be reduced to a level dictated solely by the current repairs, modernization, and operating reserve, which amounts to 20.6%.

Combination of repair jobs raises even more the imbalance factor, which reaches a value of 2.05. Furthermore, an extra throughput capacity of the communications between the systems is needed for the stations to help each other during an emergency.

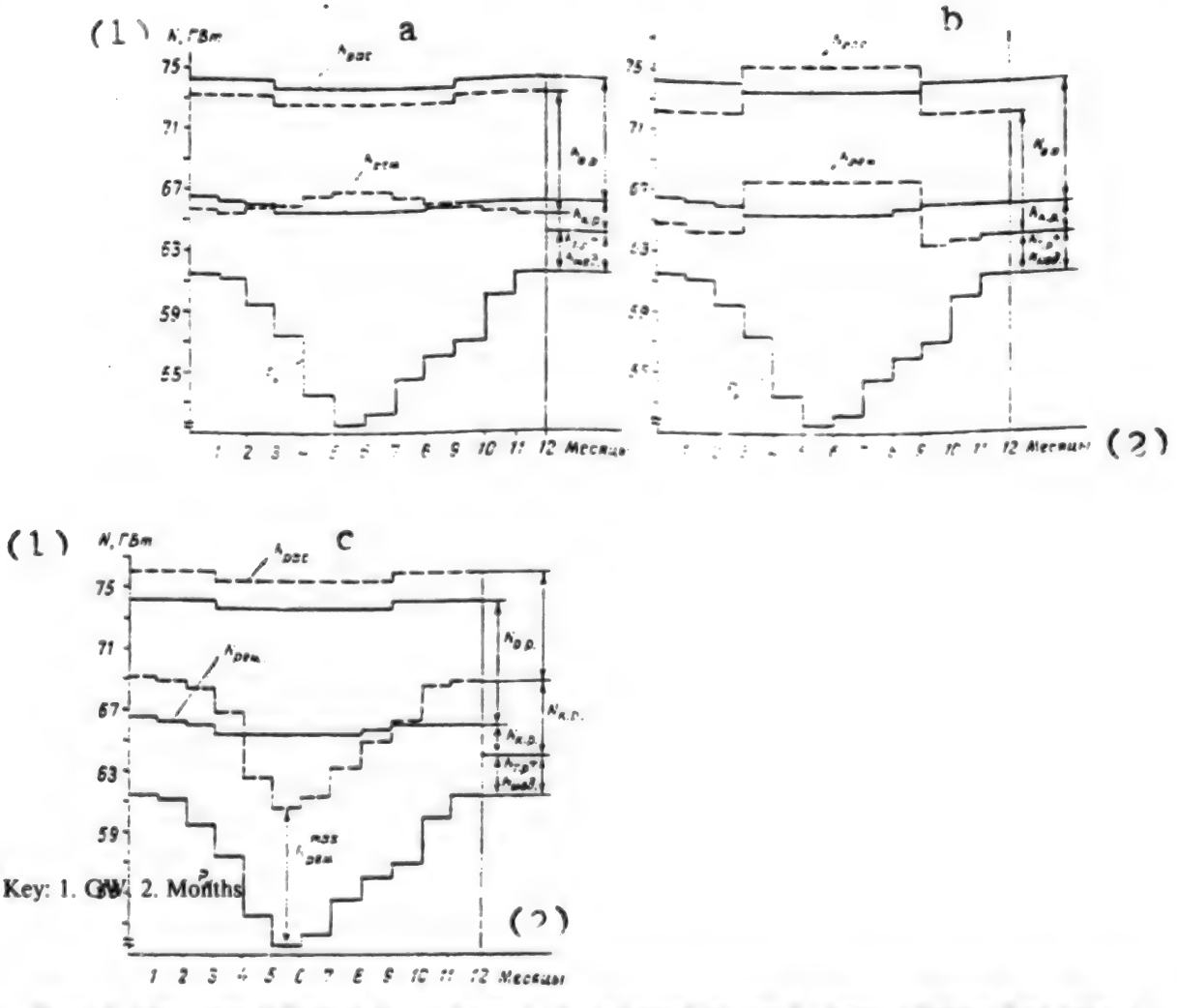

Key: 1. GW 2. Months

Figure 1. Alternatives of Optimal Repair Areas: a - in an Isolated System; b - Systems Helping Each Other; c - Limit Placed on Maximum Repair Levels; P_H - Monthly Maximum Chart; $N_{o.p.}$ - Operating Reserve; $N_{k.p.}$ - Reserve for Major and Intermediate Repairs; $N_{k.p.}+N_{mod.}$ - Reserve for Current Repairs and Modernization

Optimization of the repair charts, or the configuration of the repair area, with the purpose of reducing the overall reserve is possible in such cases where there are no restrictions on the organization of the repair process. Restrictions include:

—the number of units repaired at the same time;

—the overall equipment capacity N_{pem}^{max} placed in repair at the same time.

Calculations reveal that the first two [as given] restrictions, taken within reasonable limits, have almost no influence on the overall repair chart, although they alter the sequence of repair jobs. The third [as given] restriction, which indirectly represents the abilities of the repair enterprises, directly impacts the distribution of repair jobs. In order to achieve a maximum reserve of 20.6%, the maximum level of major overhaul in June should be 12,300 MW. Gradually making this restriction more stringent, it is first necessary to abandon the combination of repair jobs and then the optimal distribution of repair jobs within the year, replacing it with the compulsory distribution (broken line N_{pem} in Fig. 1c). As a result of introducing this restriction, the repair job imbalance factor is reduced and there is an increased need for power reserve.

When the permissible maximum major overhaul is reduced from 10,800 to 6,500 MW, the reserve requirement increases from 23.4 to 25.6%, while the imbalance factor decreases from 1.78 to 1.08, i. e., the major overhaul is almost uniform in its performance (Fig. 1c).

For our example, the relationship between the necessary overall power reserve $N_{p.\Sigma}$ and the restriction on the overall level of maximum repairs is shown in Fig. 2.

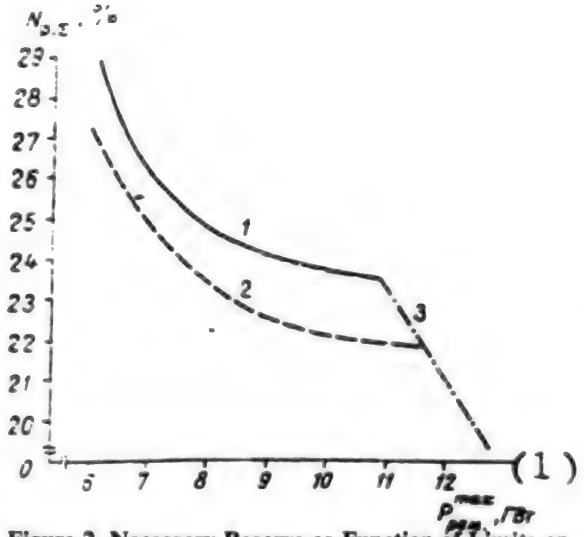

Figure 2. Necessary Reserve as Function of Limits on Repair Jobs: 1 - Not Counting Changes in Composition of the Units; 2 - Counting Changes in Composition of the Units; 3 - Counting Power Transfers When Stations Help Each Other

Key: 1. GW.

When limits are placed on the overall repair process, the alternative to increasing the power reserve is either increasing the capabilities of the repair enterprises or rationalization of the repair jobs, involving a decrease in the repair norms (reducing the duration of repairs and increasing the time between repairs).

In order to estimate the influence of the norms, calculations were made for a 10% reduction in duration of repairs. The findings show that a 10% decrease in the repair norms reduces the required reserve by 1-2% (depending on the level of the restrictions).

Conclusions. The investigations and calculations reveal that optimization of the planned repair jobs enables a substantial reduction in the requirement for overall power reserve of the system. However, this is purchased at the price of a significant rise in the imbalance factor of the repair process. Achievement of optimal repair charts (in terms of reliability) is prevented by the limited capacities of the repair enterprises and their limited ability to perform repair in a nonuniform manner. Further studies are needed to find optimal ways of resolving this conflict.

Bibliography

1. "Spravochnik po proyektirovaniyu elektroenergeticheskikh sistem [Handbook for design of electric power systems]," ed. by S. S. Rokotyan, I. M. Shapiro, Energiya, M., 1985

2. Goldenberg, F. D., "Optimizatsiya energeticheskikh sistem i ikh elementov [Optimization of power systems and their elements]," Shtiintsa, Kishinev, 1986, pp 93-99

UDC 621.311.25:621.039<<71>>

Role of Nuclear Electric Power Plants in Electric Power Industry of USSR

907F0112 Moscow ELEKTRICHESKIYE STANTSII in Russian No 12, Dec 89 (signed to press 16 Nov 89) pp 9-13 (manuscript received 8 Jan 90)

[Article by Doctor of Technical Sciences V. V. Yershevich and Candidate of Technical Sciences V. Ya. Peysakhovich, Energosteproyekt]

[Excerpts] [Passage omitted] The reexamination of the Energy Program that is now in progress has been invoked to answer a number of pressing questions, the major one being at what pace to continue development of the nuclear power industry, and what might be the consequences to Soviet economy of drastically downscaling the construction of nuclear electric power plants.

To draw attention of the power engineering community to problems of nuclear power and to clarify the position of the nuclear power industry, the All-Union Scientific and Technical Society of Power Engineers and Electricians imeni G. M. Krzhizhanovskiy (VNTOE) has conducted a survey by questionnaire.

The questionnaire contained six multiple-choice questions:

1. If construction of nuclear power plants is canceled in your territory, what energy sources could replace them?

2. Do you consider it possible to use other sources of energy to compensate for reduced nuclear power generation?

3. In case of incomplete compensation for the output of nuclear power plants by other sources of energy, what might be the consequences for your territory?

4. If nuclear sources of heat supply have been provided in your territory, what heat sources might replace them in case of canceled construction?

5. Would it be advisable to shift construction of nuclear electric plants and nuclear heat sources from your territory to another, and if so, which?

6. Your estimate of possible levels of production of energy by nuclear electric power plants throughout the nation in the year 2000, and of heat output from nuclear sources of heat supply.

Respondents were asked to indicate their choice and give a quantitative or qualitative evaluation of their response.

In all, 42 questionnaires were sent out to republic and municipal boards of the VNTOE, of which 31 were answered. Analysis of the results (Table 1) shows that there were no objections to development of nuclear power in territories covered by six questionnaires (the Kola, Kalinin, Kursk, Rovno, Smolensk and Yaroslavl regional boards).

Table 1

Item	Positive attitude toward building AES	Negative attitude toward building		Alternative to building AES				Alternative to building nuclear sources of heat					
		AES	AES in their own territory	Fossil fuel plants		Hydroelectric and unconventional sources	Transmission of electric power from another territory	Large boiler houses		Electric heat supply		TETs	
				coal	gas			gas	coal	city	rural	gas	coal
Number of questionnaires sent.....42													
Responses.....31	6	11	4	4	14	10	7	7	2	2	1	6	1
Republic boards of VNTOE													
Ukrainian		+		+	+	+	+	+	+	+		+	+
Moldavian	Construction not planned				+								
Latvian	Construction not planned												
Georgian		+			+	+							
Azerbaijan	Construction not planned				+	+		+					
Kazakh		+		+								+	
Turkmen	Construction not planned												
Kirgiz	Construction not planned												
Regional boards of VNTOE													
Donbass			+	+	+			+	+				
Rovno	+										+		
Khmelnitskiy		+			+	+							
Krymsk		+					+						
Dnepropetrovsk			+		+	+							
Kola	+			+	+	+							
Bashkir			+		+	+	+	+					
Chelyabinsk	Construction not planned						+						
Kalinin	+					+							
Leningrad		+			+	+	+	+		+		+	
Krasnodar	Construction stopped												
Yaroslavl	+												
Kursk	+												
Smolensk	+												
Volgograd			+				+					+	
Voronezh		+						+					
Territorial energy administrations, etc.							+	+				+	
Gorenergo		+											
Kostromaenergo		+			+								
Saratovenergo		+			+							+	
Ivenergo	Nuclear heat source												
Latvglavenergo	Construction not planned												
Ural Science Center		+			+								
Beloyarsk AES	Data not available												

In this context, it was noted that the detrimental environmental impact of nuclear power sources is much less than that of fossil-fuel sources. It was acknowledged that there is no complete alternative to construction of nuclear electric power plants in some territories. An opinion was expressed that building nuclear electric power plants would be effective in regions of expensive fuel by displacing fossil fuel with nuclear energy.

A negative attitude toward development of nuclear power was reflected in 15 questionnaires. The remaining respondents abstained from specific answers, but in most cases expressed a negative attitude in follow-up inquiries.

The survey showed that most public representatives are opposed to construction of nuclear electric power plants in heavily populated territories of the nation until a new generation of reactors has been built with enhanced radiation safety. New options for energy supply of territories must undergo expert review with respect to social, scientific, engineering and ecological criteria with enlistment of a wide range of specialists and the public.

Most of those surveyed propose construction of gas-fired condensation electric power plants and TETs, and also (to a lesser extent) hydroelectric plants and the use of unconventional sources.

However, the inertia of the large-scale nuclear program continues to maintain rather large power figures for nuclear electric plants in a number of directive and planning documents. For example, an article by N. F. Lukonin mentions a level of development of nuclear electric power plants of 110-120 million kW expected by the year 2000 (TEPLOENERGETIKA, No 12, 1988).

Analysis of the actual course of introducing capacities and constructing nuclear electric power plants with allowance for the position of the public, local agencies, and also the results of the survey shows that the total capacity of nuclear electric power plants in the USSR by the end of the century will be no more than 60-70 million kW, and production of electric energy in these plants will not exceed 400 billion kWh, i.e., the increase over 1985 will be by a factor of less than 2.5, rather than the figure of 5-7 that had been planned. The figure that is most accessible for verification—the actual introduction of nuclear electric power plant capacities for the 12th 5-Year Plan—will be less than 15 million kW, i.e., little more than one-third of the level planned in 1986 (41 million kW).

This confirms particular decisions that have already been made to reduce the nuclear program. It has been decided to curtail construction of the Odessa and Minsk nuclear TETs, and the Azerbaijan and Krasnodar nuclear electric power plants. The Armenian Nuclear Electric Power Plant has been shut down. Planning and investigation has been stopped, pushing back the deadline for introducing capacities at the Georgian, Far Eastern, Latvian and Belorussian nuclear electric power plants. Rated capacities have been limited for a number of nuclear electric power plants (Chernobyl, South Ukrainian, Balakovo, Zaporozhye, Smolensk, Ignalina, and others). [passage omitted]

What are the possible alternatives to development of nuclear power?

Let us try to understand just what is meant by a cut in nuclear electric plant capacities by 40 million kW (from 100-110 to 60-70 million kW, which corresponds to a drop in electric energy production by 260 billion kWh).

Theoretically, this amount of energy could be generated by fossil-fuel electric power plants.

For purposes of comparison, we point out that the generation of electric energy by all State Regional Electric Power Plants (GRES) of the Ekibastuz Fuel-Energy Complex (ETEK—4 x 4,000 MW) will be less than 100 billion kWh, and by the first two Berezovo GRES (2 x 6,400 MW) of the Kansk-Achinsk Fuel-Energy Complex—only 80 billion kWh. Compensation for the stated cut in the nuclear program will necessitate the additional inclusion of 90 million metric tons of coal equivalent [having lower heat value of 7,000 kcal/kg] of fossil fuel in the fuel balance of electric power plants. This corresponds roughly to the annual level of extraction of energy-quality coal in the Donetsk coal fields. Additional inclusion of coal on such a scale in the balance for 11-12 years to the end of the century is unrealistic, as the previously assumed quotas of increase in the use of coal in the electric power industry are not now being met. Besides, neither the equipment now in use nor that currently proposed for coal-fired electric plants corresponds to today's requirements with regard to ecological parameters.

Compensation for the stated reduction in capacities of nuclear electric plants by additional construction of hydroelectric plants is impossible, even in theory. This would require construction of 11 plants like the Bratsk Hydroelectric Plant. In the European part of the nation, where the compensation for reduced nuclear plant capacities is needed, there are no effective dam locations for high-power hydroelectric plants, but even in the eastern part of the nation, prospective dam sites give no hope for building such a number of plants with unit power close to that of the Bratsk facility. Moreover, because of the high capital intensiveness and duration of construction, it would take a long time to realize such a program. Besides, transmission of such an amount of energy to the European part of the nation over a distance of 4,000 km in the required time frame is not feasible. And we cannot fail to consider the negative public opinion with regard to hydroelectric plant construction, which leaves this option out of the question.

Even less realistic are proposals for using unconventional energy sources: wind power, solar, geothermal, biomass, and the like. The realistic prospective power range for wind turbines is from 250-300 to 1,000 kW. Wind-driven electric power plants have no guaranteed energy resource, a low number of hours of utilization of

capacity (2,000-3,000 h/yr), and require almost total backup, which makes them ineffective for European territories of the nation. Wind farms require considerable allocations of land, which is also detrimental to their characteristics. Extensive introduction of a program of building wind-driven electric plants is also being delayed by machine-building capabilities. In this regard, their fraction in the total capacity of electric power plants of the nation will not exceed 1 percent in the foreseeable future.

Of all unconventional sources, only tidal hydroelectric plants and orbiting solar electric power stations correspond to nuclear facilities in the necessary scales of energy production. However, such plants will not be making an appreciable contribution to the fuel-energy balance of the nation for the next 20 years.

The only resource that is capable to a limited extent of compensating for the reduction in the nuclear program of the next 10-15 years is natural gas. However, the actual situation as regards natural gas is such that at the decreasing rates of increase in the recovery of natural gas even in the near future, there will be a rapidly increasing demand for gas by non-energy consumers, where gas is used much more efficiently: household use, considering the increase in housing construction and the need for improving the ecological situation in cities, where coal-fired boiler houses have been built and operated until now; transportation, considering the difficulties of providing the nation with engine fuel under conditions of stabilization, or even a decrease in petroleum recovery; chemistry, which uses gas as a raw material for producing highly effective goods.

As implied by the foregoing, not a single one of the available resources is capable of compensating for the stated reduction in nuclear power.

One way to reduce the aforementioned electric energy shortage caused by cutting back the nuclear program may be to reduce the demand for electric power. Recently there have been frequent references to Western experience in conserving electric energy, apparently so effective that it has been able to stem the increasing demands for electric power. As shown by analysis of report data over the past 10 years (1978-1987), the world production of electric energy has increased on average by 3.7 percent per year (by 3.8 percent in the USSR). [passage omitted]

Numerous calculations done for a variety of conditions of development of the national economy of the USSR show that solution of the formulated economic, social and ecological problems necessitates a continued increase in the production of electric energy at a pace corresponding roughly to what has been attained: at least 3-4 percent per year with mandatory implementation of an ambitious program for conservation of electric energy. Otherwise, the stated scales would have to be drastically increased, as the problems facing our nation demand additional electric energy. It is needed by new industrial enterprises with progressive technologies (e.g., those built in cooperation with other nations), on many steps to improve the ecological situation (introduction of electric power and heat supply on the shores of Baikal), in an extensive program for development of housing construction, and so on.

Under these conditions, the following guidelines should be applied to options for developing electric energy production in the near future:

Accelerated construction of Berezovo GRES-1 and -2 of the Kansk-Achinsk Fuel-Energy Complex, and the Ekibastuz GRES-2 and -3, utilizing surplus coal resources, and also 1,500 kV DC power transmission lines between Ekibastuz and Moscow, and between Itat and Ekibastuz;

Involvement of added resources of natural gas with construction of a series of TETs in the European part of the nation, simultaneously solving heat supply, social, and economic problems, and also of individual GRES by way of an exception in peripheral critical regions (the Transcaucasus, Latvia, the Crimea), where the reliability of energy supply is simultaneously being improved;

Construction of two large coal-firmed GRES (using Kuznetsk or improved Kansk-Achinsk coal) in the Ural-Povolzhye region, which in the initial stage of service may use natural gas, considering that the additional natural resources of the European zone (Donetsk, Pechora and Moscow coal) may not be realized in practice for in the next 15 years, particularly with allowance for the increasing demands of ecology.

It would also be advisable to consider the possibility of displacing Kuznetsk coal from existing TETs and those to be built over the next 10-15 years by supplying them with natural gas and using the coal that is saved for new condensation power plants, which would improve the ecological environment in cities served by TETs, and improve the efficiency of using additional natural gas resources. [passage omitted]

UDC 624.073.2:639.376

Calculating Primary Band of Variable Rigidity

907F0077A Yerevan IZVESTIYA AKADEMII NAUK ARMYANSKOY SSR: SERIYA MEKHANIKA in Russian Vol 42, No 1, Jan-Feb 89 p 56

[Annotation by N. F. Kakosimidi: "Calculating the Primary Band of Variable Rigidity in a Base Having Finite Depth, and Possessing Creep"]

[Text] The article examines the two-dimensional problem of calculating the primary band of variable rigidity in a base having finite depth, the material of which base satifies the prerequisites of the Boltsman-Bolter theory of elastic heredity. The reaction pressures of the base are investigated as the sums of the reaction pressures which correspond to the elastic-momentary problem and the increments of the pressures generated by creep. The latter, which are unknown, are determined from their self-balancing condition as well as the condition of contactability of the band and the base, which condition occurs in integral form at individual sections of the contact. The solution to the calculation, which is illustrated by a numerical example, shows that creep in the base significantly effects the distribution of reaction pressures.

UDC 621.37/.39.019.3

Some Aspects of Reliability of Flexible Automated Production

Moscow NADEZHNOST I KONTROL KACHESTVA in Russian Oct 89 [signed to press 18 Aug 89] pp 40-46 [MS received 01 Nov 89]

[Article under the "Issues of Reliability Assurance of Industrial Production" rubric by L. G. Dubitskiy]

[Text] Flexible automated production (FAP) should provide:

single, small and medium series manufacture (in certain cases, large series as well) that makes it possible to achieve products with the individualized qualities of each item;

an "end-to-end" automated design process, control over the setup of the production system, the production, and the technical handling of all component parts and of the product as a whole, which is what comprises an integrated production;

a human-free and grouped technology with round-the-clock cycle, high production rate and maximum concentration of operations, robotization, and adaptive numerical program control to handle the design and production tasks;

high reliability and precision of the design, engineering, measurement- inspection, diagnostic, testing, and other equipment;

manufacture of products of high engineering stature, requisite quality, dependable and competitive, economically effective, ecologically clean, and possessing other attributes satisfying to the consumer, with strict observance of the time table for the set delivery volumes.

The implementation of all the above functions is done during the development of the FAP on a unified mathematical foundation [2], in which are also comprised mathematical relations that evaluate (predict) the product reliability criteria. These relations, however, are extremely general in nature and of limited applicability in the choice of rational ways of reliability assurance of, for example, microelectronic items. In [3], the requirements are formulated for extremely large scale integrated circuits: on the level of 10^7 p-n junctions per chip the failure rate should be no higher than 10^{-9} 1/h for an annual shipment volume of up to 10^6 1/year. Roughly speaking, not a single microcircuit out of the semiannual shipment volume should fail.

These demands on the reliability of FAP products necessitate a scrutiny of the components of reliability, i. e., the causes of failure as related to particular components of the product item and the conditions of their manufacture and use. On this basis, steps can be defined for assurance of reliability, which is the subject of the present article.

First of all, let us mention the primary causes of failure as emerge from the foregoing list of FAP functions.

1. Individualization of the functional qualities of each product item allows flaws to become evident in the debugging process, due to inadequate understanding of the qualities during use.

2. The "end-to-end" automated process gives rise to flaws because the data as to the properties of the materials and complementary parts adopted during the computerized design process are not identical to those actually used during manufacture; the data as to the factors of influence, the conditions of usage, and the stresses during operation, as adopted during the design process, are not identical to those actually occurring during production and during usage; and the data as to the characteristics of the design, engineering, measurement-inspection, diagnostic, testing, repair and other equipment used to develop the entire chain of the end-to-end automated process are not identical to those actually used in the development, production, and servicing (and also because of failures in this equipment).

3. The grouped technology gives rise to failures because of differing qualities of product items within the particular group, not detectable by the existing quality inspection system.

4. Robotization of production and use of automatic machinery with numerical program control gives rise to failures because of software flaws (malfunctions) and inadequate promptitude in adapting the programs to the changing qualities of materials and manufacturing conditions.

Hence, it follows that the unreliability of FAP products is explained by two groups of factors, stationary and nonstationary. A classification of failures and methods of reliability assurance of FAP products is given in Fig. 1.

The first group pertains to the instability of the qualities of the products and their working conditions, which in a statistical sense are described by stationary random processes over time. This group is characteristic of any kind of production, and not just FAP. The failure rate of FAP products is in fact much lower than that of nonautomated production products. Investigation of the causes of failures and their statistics by the methods of physical (nondestructive inspection, physical-technical fault analysis) and technical diagnostics [4, 5], by carrying out tests and analysis of data from the realm of product usage provides the starting data for calculation (assessment) of reliability by traditional methods [6, 7]. In FAP products, certain "inherited" qualities occur very often, making it possible to use methods of accelerated testing in ordinary and excessive duty [8, 9]. In some instances, dimensional and other factors of product similarity may be included in the reliability assessment, making it possible to employ methods from the theory of analogy [10]. Statistical modeling of faults

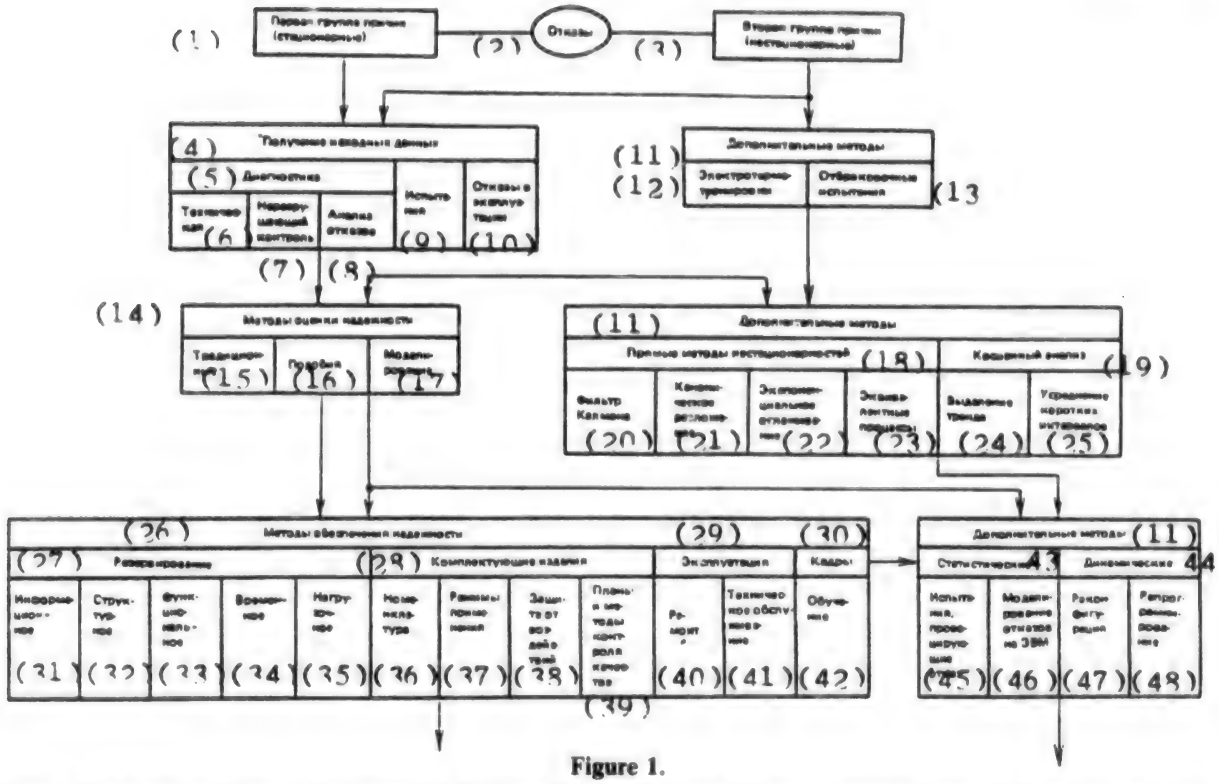

Figure 1.

Key: 1. First group of factors (stationary) 2. Failures 3. Second group of factors (nonstationary) 4. Production of initial data 5. Diagnostics 6. Technical 7. Nondestructive inspection 8. Fault analysis 9. Testing 10. Failures during use 11. Supplementary methods 12. Electrothermal conditioning 13. Rejection testing 14. Reliability assessment methods 15. Traditional 16. Analogy 17. Model investigation 18. Direct methods of transients 19. Indirect analysis 20. Kalman filter 21. Canonical expansion 22. Exponential smoothing 23. Equivalent processes 24. Trend identification 25. Averaging of short intervals 26. Reliability assurance methods 27. Redundancy 28. Complementary products 29. Service 30. Personnel 31. Information 32. Structural 33. Functional 34. Temporal 35. Workload 36. Product spectrum 37. Usage conditions 38. Protection against external effects 39. Quality inspection plans and methods 40. Repair 41. Maintenance 42. Instruction 43. Static 44. Dynamic 45. Fault-provoking tests 46. Computer modeling of faults 47. Reconfiguration 48. Reprogramming

and situational modeling of fault precursors are coming into general use in reliability assessment [11].

Thus, on the whole, there is a sizeable arsenal of methods and programs for assessment of the reliability of FAP products as conditioned by the first group of faults. The control of faults produced by these causes usually comes down to employing redundancy (informational, structural, functional, temporal, and workload) conformable to the choice of complementary items and their service conditions, protection against external effects, rationalization of the testing and inspection (statistical and nondestructive) plans and methods, improvement of the repair and maintenance, and better training of the work force. All of the methods are well known, though not always used in an integrated and efficient manner.

In addition, improved reliability of the process computing and measurement-inspection equipment is taking on ever increasing importance in the control of faults of FAP products. The distribution of FAP faults is characterized by the following data: 38% stem from the procurement systems (including power, tools, blanks), 27% the control systems (including computers), 7% the power drive, and 28% the inspection systems, 10-12% of which are faults of the quality inspection systems, as a result of which unfit products may get to the consumer.

The second group of faults (see Fig. 1) is largely due to the unsteady nature of production under FAP (a diagram is shown in Fig. 2, where $\lambda(t)$ is the rate of FAP product faults; t is the time of operation of the FAP; t_i' is the time of change in the characteristics; t_i is the peak fault rate during setup; t_i'' is the time when the fault rate reaches a constant segment; t_p is the onset of FAP equipment trouble involving service life. The unsteady process is

due to "bursts" of setup flaws (as it were) on the fault rate curve as the next group of products with individualized qualities is commenced. "Setup" flaws occur in any kind of production, but is the process continues for a lengthy time, manufacturing products of identical type, then after setting up the production with use of trial runs, electrothermal conditioning, and other kinds of reject testing it is possible to avoid supplying products to the consumer with a high rate of flaws. In FAP, the frequent change in characteristics of the products, which is necessary to individualize their qualities, requires that special steps be taken to avoid supplying products with a high rate of flaws from the setup period.

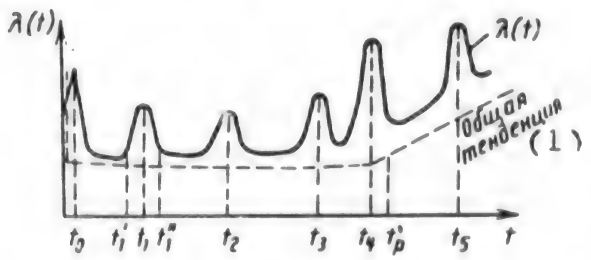

Figure 2.

Key: 1. General trend

The existing data show that the "setup" bursts in the fault rate may exceed the mean level by a factor of 10-100. The characteristic law in the distribution of such faults is a growth in their maximum rate, a relative increase in the duration of the burst, as compared to diminishing time of setup of the FAP. Therefore, the "setup" causes of flaws (for conventional production, these are transient compared to the duration of the production of the given type of product) may turn into a very permanent factor of unreliability of FAP products. As the "flexibility" of the FAP increases (i. e., the time to start a new type of product decreases), the ratio between the maximum and the average fault rate grows.

In order to assess the reliability of products as conditioned by "setup" flaws during adjustment of the FAP system it is necessary to employ specific methods of analysis of nonstationary random processes [12]. These methods (see Fig. 1) can be divided into direct algorithms for analysis of nonstationary processes, using the appropriate predictors (on the basis of the Kalman filter, canonical expansion, exponential smoothing), and indirect algorithms which employ a preliminary transformation of nonstationary random processes into equivalent stationary ones (by identification of the trend, by averaging over short time intervals, etc.) with subsequent statistical classification (on the basis of identification systems [13]).

Thus. in order to assess the reliability of FAP products it is necessary to assess the components dependent on both groups of failures.

Assurance of reliability for such products requires efficacious control of "setup" flaws, one promising solution being combined use of special kinds of testing and simulation modeling (see Fig. 1).

Special kinds of testing are carried out by means of so-called "tunnel" chambers, through which each finished product is sent. In the chamber, this product may be subjected to an action that provokes a failure if the item has a latent defect. For example, if there are blind cracks in a brittle material, then these cracks under thermal stress in the tunnel chamber may turn into through cracks, which will be found during the inspection for tightness, and such product will be rejected. Other kinds of testing in the tunnel chamber may have multiple factors, simulating the most damaging conditions of usage. For example, for cold-brittle materials, this may be a combination of cooling and impact. During or after going through the tunnel each product is checked by measurement of parameters or by nondestructive inspection. Simulation modeling makes it possible to calculate, for the given item (on the basis of measurement of parameters after going through the chambers), the likelihood of a failure over the established period and, thus, to assess its reliability.

The methods of reconfiguration and reprogramming may be used separately or jointly to ensure freedom from failure (see Fig. 1). The essence of the method of reconfiguration consists in altering the structure of the product on a given command; for example, certain of its components are disabled, and in their place other components or redundant assemblies are used. The product may remain entirely serviceable or perform the same functions with less efficiency (more slowly, for example), or it may cease to perform certain auxiliary operations (for example, register its operating time). In the method of reprogramming, the operating program of the product, such as the sequence of implementation or the distribution of functions among the assemblies, is changed on a given command.

The main point in the assurance of fault resistance of products is the formation of the signals that are used for the reconfiguration or reprogramming. Two fundamentally different approaches to the formation of these signals exist. The first approach (let us call it diagnostic) involves a periodic diagnosis of the operating product in order to discover a faulty component, the presence of which is what generates the signal for reconfiguration or reprogramming. We may note that, in this approach, there is always a certain time during which the normal functioning of the item is interrupted on account of failure of a particular component. Of course, a sophisticated diagnostic system is able to reduce this time to a reasonable minimum, but in theory such product has flaws, though not lengthy in nature.

The other approach is set forth in [5, 14] and involves determination of the precursors of the primary possible causes of failure. By precursor of a failure we mean the physical effects that occur with high probability during a

certain time prior to commencement of the failure. In our lifetime, the precursors of earthquakes, thunderstorms, and other natural phenomena have become well known. An extremely effective precursor of many kinds of failures (mechanical, thermal, radiation) are exoemission effects, which involve the emission by the substance of thermal, luminous, acoustic, or corpuscular fluxes that are formed upon release of internal energy during the initial phase of failure of the material. A detailed exposition of acoustoemissions (the "cry of sheet steel") which occur shortly before fatigue and other kinds of failure of metals and semiconductors is presented in [15].

Thus, the assurance of reliability of products manufactured by FAP requires adoption of a number of special measures that should be provided as early as the development of the product design, the engineering, and the operating instructions. Only in this way can all positive effects from the adoption of FAP be achieved.

It is advisable to create a specialized group of normative and methodological documents for the above faults in order to ensure reliability of FAP products.

The Western experience [16] testifies that, in addition to the usual measures for reliability assurance of FAP, supplementary measures are adopted, as specified by documentation of the respective companies. Such regulation is also provided by international standards on quality systems.

Bibliography

1. Popov. Ye. P., "Robotekhnika i gibkiye proizvoditelnyye sistemy [Robot engineering and flexible production systems]," Nauka, M., 1987, 192 pp.

2. Meshkin, N. P., Shchegolev, V. A., "Matematicheskiye osnovy tekhnologicheskoy podgotovki gibkogo avtomatizirovannogo proizvodstva [Mathematical foundations of the engineering setup of flexible automated production]," Izd-vo standartov, M., 1985, 256 pp.

3. "Mikroelektronika: Ucheb. posob. dlya vuzov [Microelectronics: a textbook for technical colleges]," ed. by L. A. Koledov, Book 5, I. Ya. Kozyr, "Quality and reliability of integrated microcircuits," Vysshaya shkola, M., 1987, 144 pp.

4. Berdichevskiy, B. Ye., Dubitskiy, L. G., Sushintsev, G. M., Ageyev, A. P., "Nerazrushayushchiy kontrol elementov i uzlov REA [Nondestructive inspection of radio electronic components and subunits]," Sov. radio, M., 1976.

5. Berezhnoy. V. P., Dubitskiy, L. G., "Vyyavleniye prichin otkazov REA [Identification of radio electronic failure causes]," ed. by L. G. Dubitskiy, Radio i svyaz, M., 1983, 226 pp.

6. "Metody rascheta nadezhnosti detaley i uzlov bytovykh mashin i priborov: Uchebnik dlya vuzov [Methods of calculation of the reliability of household machine parts and subunits: a textbook for technical colleges]," ed. by Ye. A. Panfilov, Legkaya industriya, M., 1979, 320 pp.

7. "Nadezhnost tekhnicheskikh sistem: Spravochnik [Reliability of technical systems: a handbook]," ed. by I. A. Ushakov, Radio i svyaz, M., 1985, 608 pp.

8. Perrote, A. I., Kartashov, G. D., Tsvetayev, K. N., "Osnovy uskorennykh ispytaniy radioelementov na nadezhnost [Principles of accelerated reliability testing of radio components]," Sov. radio, M., 1968, 224 pp.

9. Kartashov, G. D., "Forsirovannyye ispytaniya apparatury [Excessive- duty testing of equipment]," Znaniye, M., 1986, pp 51-106.

10. "Nadezhnost i effektivnost v tekhnike: Spravochnik [Reliability and effectiveness in engineering: a handbook]," Mashinostroyeniye, M., 1987, 280 pp.

11. Aleksanyan, I. T., Krivoshapko, V. M., Rubanik, Yu. T., "Simulation of electromigration faults in integrated circuit components by computer," ELEKTRONNAYA TEKHNIKA, Series 8, Issue 6, 1976, pp 31-39.

12. Vasilyev, B. V., "Distantsionnoye upravleniye nadezhnostyu i effektivnostyu radioelektronnykh ustrostv [Remote control of reliability and effectiveness of radio electronic devices]," Radio is svyaz, M., 1983, 224 pp.

13. Bulkin, M. A., Gorelkin, Ye. N., Dubitskiy, L. G., Rozinkov, N. S., Solyar, V. G., "Use of methods of pattern recognition in electronic product quality control systems," ed. by L. G. Dubitskiy, OBZORY PO ELEKTRONNOY TEKHNIKE, Series 8, Issue 3 (366), Izd. TsNII "Elektronika", M., 1976, 76 pp.

14. Dubitskiy, L. G., "Discovery of the causes and precursors of radio electric product failures," "Fizika otkazov [The physics of failures]," Nauka, M., 1981, pp 5-21.

15. Kiryakin, A. V., Zheleznaya, I. L., "Akusticheskaya diagnostika uzlov i blokov REA [Acoustic diagnostics of radio electronic subunits and assemblies]," Radio i svyaz, M., 1984, 192 pp.

16. Froman, B., Lezazh, Zh.-Zh., "Flexible manufacturing systems in machining," (trans. from French by N. A. Shurova), ed. by V. A. Leshchenko, Mashinostroyeniye, M., 1988, 120 pp.

UDC 62-192

The Prospect for Introduction of Established Reliability Criteria for Industrial Robots

907F0105A Moscow NADEZHNOST I KONTROL KACHESTVA in Russian Sep 89 [signed to press 20 Jul 89] pp 60-62 [MS received 06 Nov 89]

[Article by S. Vuchkov, Bulgaria]

[Text] Recently, the issue of using established reliability criteria (ERC) for industrial robots made in Bulgaria has become urgent.

Questions regarding ERC for manufactured articles and their parts, the subject of lengthy and sharp debate among Soviet reliability experts [1- 3], have also affected Bulgarian industrialists.

In our opinion, in connection with the subject of ERC for manufactured articles it is necessary to pay heed to three major aspects which characterize the industry of the socialist countries, and especially Bulgaria.

First, at present ERC are not an item of standardization, i. e., they are not included in the list of standardized reliability criteria.

Second, no methodology has been worked out for our special setting and we have no personal experience with the practical introduction of ERC.

Third, there are very weighty arguments against the use of ERC in industry, while the proof mentioned in support of ERC is sometimes not convincing.

The transition to such major practical step as the introduction of ERC requires a deep and thorough analysis of a number of methodological, technical, and economic issues. In the absence of serious and well reasoned discussion of many of the problems which occur, the practical introduction of ERC instead of improving the reliability of industrial products may lead to the directly opposite effect.

After a study of the Western experience and the operating conditions of the Bulgarian industry, we may formulate the following factors standing in the way of mandatory adoption of new criteria of the ERC type.

1. The economic factors which favor the adoption of ERC have not been developed, nor have economic stimuli been created for their introduction.

2. The prospect of using ERC for many articles, including industrial robots, has not been proved.

3. A methodology has not been worked out and there are no data on the basis of which it would be possible to assert, with the necessary certitude and authenticity, that greater efficiency and higher reliability are achieved by the adoption of ERC for specific articles, including industrial robots, as compared to the use of (for example) traditional statistical norms for product reliability.

4. The theoretical foundations have not been laid for the analysis and experimental evaluation of ERC of products, and the area of application of ERC for different types of products has not be established.

5. The parameters of the basic processes of degradative kind (wear, aging, buildup of defects, etc.) in industrial robots have not been investigated, i. e., the physical premises for possible use of the hypothesis of shifting the distribution of the operating time till failure have not been analyzed.

6. The recommendation for practical adoption of product ERC thus far has not been matched with a comprehensive and well reasoned strategy (or group of strategies) for ensurance and enhancement of the product reliability level, including that of industrial robots and their components, during all phases of the life cycle.

7. The conditions and a unified methodology and organization of the use of ERC in the CMEA member nations have not been created.

8. There are no ERC in the other industrial nations of Western Europe, the United States, or Japan, even though different forms of warranty protecting the interests of the customer exist here.

9. A methodology of standardization for use of product ERC, including those of industrial robots, has not been elaborated.

10. From the semantic viewpoint, given the dynamics of development of the concept of ERC, the content of this term at present requires appropriate clarification.

It is not hard to find other issues and problems of secondary order of importance in connection with the adoption of ERC.

At present, advocates of ERC envision a comprehensive introduction of these, but regrettably they do not properly answer all problems which might occur. Given the present principles of science and practice, one must not first look for quick means of adoption of ERC, and then prove their utility at a later date. Clearly, the reverse procedure should be followed.

But even if a strategy were fully developed for reliability enhancement by using product ERC, another cardinal issue would arise: would it not be more efficient for the national economy to employ several strategies, and not just one, however good, for the enormous diversity of industrial products? What would be the results in the improvement of industrial robot (for example) reliability when it is possible to choose not one, but several competing strategies or groups of strategies, which also make use of statistical reliability criteria?

It is difficult to say at present why product ERC can replace all the other reliability criteria. A consensus is emerging that if product ERC be connected with the warranty characteristics, and not set against the other reliability criteria, then it would be possible to incorporate them in proper manner in the general group of product reliability criteria. In such case, it would be possible to study the effectiveness of introduction of the ERC for a particular group of products for a particular time. It does not appear wise at present to hasten to adopt ERC for industrial robots. First of all, one should carefully weigh all pros and cons, and only then adopt

the new criteria. It may be observed that the critics of ERC adoption have much better arguments than those in support of it. At the same time, they do not propose rejection of ERC, but a transfer of them into the area of warranty conditions.

Bibliography

1. NADEZHNOST I KONTROL KACHESTVA, No 4, 1988, pp 45-57.

2. Gnedenko, B. V., Ushakov, I. A., "Standardization of reliability and "perestroyka" of attitudes," STANDARTY I KACHESTVO, No 7, 1988. 3. Shper, V. L., "Is this perestroyka?", NADEZHNOST I KONTROL KACHESTVA, No 7, 1988.

UDC 658.52.011.56.012.3.004.14 62-21.002.5

Flexible Production System for Machining of Body Parts

907F0104A Moscow MASHINOSTROITEL in Russian Nov 89 [Signed to press 13 Nov 89] p 17 [MS received 18 Dec 89]

[Article by L. I. Kortusov, G. G. Fedorov, N. N. Lukin, V. A. Grigoryev, and G. I. Kontarez]

[Text] The first phase of a flexible production system (GPS) has been introduced, based on four homogeneous interchangeable machining centers model IR-500PMF4. A classification scheme has been worked out for group machining of 42 kinds of body parts of aluminum and magnesium alloy, forming groups of parts that are identical in design and processing features. This allows the necessary tooling, a grouping of the technological processes, and a choice of the group fixtures and cutting tools.

The configuration of the GPS, shown in the figure, has the process equipment moving along a materials handling center 12. The transport steps (machine - materials center - processing positions) take place through the compartments of the materials center. The GPS includes: a control computer complex (UVK) SM-1420, item 8; a machining center 6, mod. IR-500PMF4; an automated transport and materials handling system ATSS SA-0.5 with stacking robot RSh-0.5, item 9; the control system MEGA-2101, item 1; roller conveyors 3 and 5 for the carrier and the box, respectively; alignment units 11 for positioning the carrier-tables during the transfer from the ATSS to the hopper of the machine tool; loading-unloading positions 10; video terminals VTA 2000-15, item 7; sectors 2 and 4 for tool setup and fixtures setup, respectively. The GPS takes up an area of 350 m^2.

The GPS is adopted in phases. This makes it possible to cut down on the time lost and greatly reduce the standstill of the basic processing equipment. In the first phase, the metal cutting equipment (the foundation of the GPS) and the ATSS were installed as independent processing

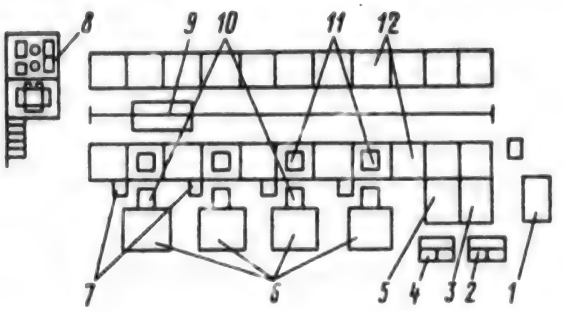

units with subsequent fabrication, installation, and introduction of processing positions and of the automated control system (ASU).

The structure of the GPS is two level. The link between the UVK SM-1420 and the control system ATSS MEGA-2101 and the peripheral controller based on the computer Elektronika-60, used to load the control programs (UP) into the BOSh CNC Mikro-8, occurs via data transmission multiplexer MPD 8529. The basic operating modes of the first phase of the GPS are: initial loading, normal functioning, reconfiguration in event of malfunction, completion of work, ATSS servicing of sectors not included in the GPS.

The basic goals for realization of the second phase of the GPS are: introduction of automated tool change, operational-calendar scheduling of the work of the GPS and the machine sectors not included within the GPS, automated correction of the UP and identification of a workpiece in the normal functioning mode, introduction of a booth-type rinsing of shavings from the workpiece, introduction of a link controller between the BOSh CNC Mikro-8 and the UVK. By virtue of performing the preparatory and concluding steps away from the machine tool, the proportion of machine time in the overall time per piece has been boosted by 10-15%, and the equipment production rate by a factor of 1.6.

The total economic impact from adoption of the GPS is 120,000 rubles.

A Turbine for Re-Engineering

907F0087A Moscow ENERGETIK in Russian No 11, Nov 89 pp 9- 10

[Article under the "Re-Engineering of the Power Enterprises" rubric by G. D. Barinberg, candidate of technical sciences, and L. S. Ioffe, engineer, Production Association "Turbine-Motor Plant"]

[Text] The production association "Turbine-Motor Plant" proposes the specially developed steam heating turbine Tp-115/125-130TP for replacement of worn and obsolete steam turbines. This turbine will be made in three modifications, which can be used effectively in the different settings of the specific power stations, dictated primarily by the thermal loads.[1] All three modifications of the turbines Tp-115/125-130TP can supply steam for

production purposes in the amount up to 70 T/h. However, if turbines of 25 MW capacity of type VPT-25-3 and VPT-25-4 with initial steam parameters of 8.8 MPa, 535-500°C, and turbines VPT-50-3 (PT-50/60-130/13) and VPT-50-4 with parameters of 12.8 MPa, 555°C, have been installed in the power stations to provide for large production workloads, it may not be possible to replace them with turbines Tp-115/125-130TP. In such cases, the association proposes installing a turbine of type PT-90/120-130/10TP, which can be developed and delivered by the association in a short time. The new turbine is created on the basis of the long-time veteran heating turbine T-110/120-130-5 with rated capacity of 110 MW.

The turbine PT-90/120-130/10TP is designed to work with live steam of pressure 12.8 MPa and temperature 555°C, but if boilers of lower parameters are still present at the power station the turbine can operate for a long time with live steam of pressure 8.8 MPa and temperature 535°C, naturally with a consequent lowering of the live steam flow rate, the electrical power, and the thermal load.

The turbine is scheduled for production in two modifications, PT-90/120- 130/10-1TP and PT-90/120-130/10-2TP, having blades of the last stage respectively 550 and 650 mm long. The first modification is more economical in heat supply duty with low steam admission in the condenser and requires less cooling water flow rate, the nominal level of which is 8000 m^3/h. It is advisable to install the first modification turbines in heat and electric supply stations (TETs) where the production and heating loads are met in a certain amount year round, including the summer season, and therefore it is possible to allow a limited turbine power in pure condensation duty (which is around 80 MW) at somewhat lower economy.

The second modification makes it possible to produce maximum electric power of 120 MW in condensation duty at rather high economy: the nominal flow rate of cooling water is 13,500 m^3/h. At low steam flow rate to the condenser during the operation of the turbine with large thermal load, the economy of the second modification turbine is somewhat less than that of the first.

For turbines of both modifications at nominal power of 90 MW, nominal live steam parameters (12.8 MPa, 555°C), and two-stage heating of the mains water, the nominal thermal heating load is equal to 75 Gcal/h and the amount of steam tapped for production is 195 T/h. The maximum heating load is 120 Gcal/h, and the maximum steam flow for production 365 T/h.

The maximum power of both modifications of turbine is 120 MW, the maximum live steam flow rate 500 T/h.

The nominal turbine power is ensured with a production steam tap of 250 T/h and no heating load, and also at a heating load of 120 Gcal/h with an appropriate production steam tap or steam admission to the condenser.

If necessary, an additional regulated steam tap of as much as 70 T/h at pressure around 2 MPa can be organized from the high pressure cylinder (HPC) outlet in the turbine.

At the maximum steam tap for production of 365 T/h, the turbine power is no less than 70 MW.

The range of change in the regulated pressure in the upper heating tap with a two-stage heating of the mains water is 0.06-0.245 MPa. It is permitted to work with a single-stage heating of the mains water, in which case the range of variation in the regulated pressure is 0.05- 0.196 MPa. The range of variation in the pressure in the production tap is 0.78-1.27 MPa.

The turbine is a two-cylinder, single-shaft unit, consisting of HPC and LPC. In the HPC there are arranged a two-rim regulating stage and 8 pressure stages, in the LPC there are 15 stages, two of which are single-rim regulating stages: one (stage 16) to regulate the pressure in the production tap, the other (stage 23) to regulate the pressure in the heating taps.

The feed water is heated mainly in an ejector, the ejector of the packings, an oil seal heater, three low pressure heaters (LPH), a deaerator of 0.59 MPa, and two HPH. Tapping of steam for the last HPH is done after the HPC, that for the other heaters is done from the tap chambers of the LPC.

The length of the turbine is 14,455 mm, the width of the turbine in the cross section of the exhaust branch is 7680 mm. The exhaust branches for blades of 550 and 650 mm, having identical outer dimensions, differ from each other in their design and in the dimensions of the parts located inside the branch.

The condenser of the turbine has a "built-in" bundle for recovery of the heat of the ventilation steam flow of the stages of the low pressure purifier of the mains or makeup water for the 550 mm blade and only the makeup water for the 650 mm blade in heat supply duty, which makes it possible to maintain high economy of the turbine installation during the heating period.

The turbine regulation system is electrohydraulic (EGSR), which in contrast with hydraulic regulation systems enables expanded functions of the automatic regulation system, as well as higher accuracy of maintaining the regulated parameters. Depending on the operating duty of the turbine, the EGSR is capable of maintaining in given limits the frequency of rotation of the rotor; the electric load (power); the temperature of the mains water in one of the heating stages or the temperature difference between the outgoing and the return mains water, which determines the constant thermal load under constant mains water flow rate, the temperature of the makeup water at the outlet from the built-in bundle of the condenser, and the pressure in the production tap.

The turbine has the option of producing additional power, thermal load, or steam flow for production by having the feed water bypass the HPH.

As compared to turbines for steam parameters of 8.8 MPa, 535-500°C, the turbine PT-90/120-130/10TP enables a fuel savings, thanks to raising the initial steam parameters and the unit power, a two-stage heating of the mains water, an increased range of pressure regulation in the heating taps, recovery of the heat of the ventilation steam flow in the built-in bundle of the condenser and increased accuracy of maintenance of the regulated parameters, as well as partial bypass of the HPH in the feed water. Compared to turbines with initial steam parameters of 12.8 MPa, 555°C, and nominal power 50 MW, the turbine PT-90/120-130/10TP provides a fuel savings by virtue of increasing the nominal power, recovery of the heat of the ventilation steam flow in the built-in bundle of the condenser, partial feed water bypass of the HPH, and increased accuracy of regulation of the parameters.

The outside dimensions of the installation with turbine, generator, and auxiliary equipment are approximately 25,000x33,600 mm, i. e., it can fit into a machine room where there are two 25 MW turbines installed, although it should have its own foundation. The turbine PT-90/120- 130/10TP is installed in the compartment of turbines VPT-50-3 and VPT- 50-4 with partitioning of the foundation.

The advisability of using individual elements of foundations of turbines VPT-50 when replacing them with the turbine PT-90/120-130/10TP can be considered in addition for the specific replacements.

Footnotes

1. Kuzyushin, V. K., Alekso, A. I., Ioffe, L. S., et al., "Power generating machines from the Production Association Turbine-Motor Plant," ENERGOMASHINOSTROYENIYE, No 9, 1988, pp 2-7.

Abstracts From 'Autometrics'

907F0055A Novosibirsk AVTOMETRIYA in Russian
No 4, Jul-Aug 89 pp 115-119

[Abstracts appearing in "Autometrics," July-August 89]

[Text]

UDC 62-507:681.326

Principles of and Algorithm for Directed Generation of Tests in PRANTsIS-TM System. G. V. Zizin, V. V. Kashtanov, I. Ye. Lobov, V. Ye. Mezhov, and Yu. A. Chevychelov, pp 3-8

This article describes the general principles of and an algorithm for synthesizing tests that have been placed at the foundation of the Test subsystem, a subsystem for automatic directed generation of test sequences that is a part of the PRANTsIS-TM logical modeling and test generation system. The qualitative comparative characteristics of the proposed algorithm relative to traditional automated test generation methods designed by using a random number generator and D-algorithm are given along with the results of using the specified algorithm when generating tests. References 3.

UDC 681.5

Graphic Method of Inputting Information About Circuit in Circuit Board CAD System. S. G. Dementyev and V. G. Selivanov, pp 9-14

This article describes a method of plotting the image of an electronic circuit on the screen of a color graphic display as well as a translator program for translating the graphic images of schematics to create lists of circuits and component names and produce documentation for the circuits developed. The general structure of the circuit board CAD is presented. Figures 4, references 16.

UDC 681.782.473:621.3.049.75

Laser Image-Reading Device for Optical Monitoring of Circuit Boards. Yu. V. Baytsurov, A. M. Itigin, V. A. Legonkov, V. V. Oborin, L. V. Pivkina, and T. N. Khatsevich, pp 15-19

This article examines the optical train and technical characteristics of a laser image-reading device for optically monitoring the quality of a circuit board conductor drawing. The experimental characteristics of the output signal of the photoreceiving unit are presented along with the interference band values as a function of the scanning reflector's turning angle. Figures 4, references 5.

UDC 621.391

Effectiveness of Algorithms for Estimating Area of Optical Image Against Noise Background. Ye. P. Nechayev and A. P. Trifonov, pp 20-22

This article presents an investigation of algorithms for estimating the area of an optical image by the method of statistical modeling on a computer. The article also presents the bounds of the applicability of the asymptotic exact expressions for the bias and scattering of the estimate that exist in the literature and that have been derived on the basis of the method of local markovian approximation. Figures 4, references 5.

UDC 771.64

Interpolation of Signals With Finite Fourier Spectrum. Computer Experiment, L. A. Ayzenberg, B. A. Kravtsov, and B. A. Shaimkulov, pp 23-28

This article describes a computer experiment in interpolating a signal with a finite Fourier spectrum (in other words, the Fourier spectra of finite signals) on the basis of a method that was previously proposed by one of the authors and that is based on a simple formula for interpolating analytical Wiener-class functions. The method may be used to eliminate noise concentrated at a specified frequency band when necessary to convert to a Radon transform on the basis of incomplete data in computer tomography and other situations. Figures 2, references 19.

UDC 62.505

Systems Identification Methods That Are Free of Strong A Priori Hypotheses. K. V. Isayev, pp 29-35

This article examines systems identification methods that are free of strong a priori hypotheses, i.e., free of a statistical hypothesis or a hypothesis regarding the separation of data into parts that do and do not contain noise. Reference functionals and complete least squares methods that satisfy the fundamental principles are proposed. Hypotheses corresponding to them are formulated. References 7.

UDC 621.391

Identification of Parameters of Model in Form of Sum of Exponential Functions Using Prony Method. O. O. Drobakhin, pp 36-41

The precision of determining parameters by the Prony method in the presence of additive noise is investigated on the basis of computer modeling. Recommendations are given regarding selecting the optimum digitization interval. The method's resolution is investigated. Table 1, figures 2, references 15.

UDC 681.3

Frequency-Selective Method of Measuring Voltage by Using Discrete Fourier Transform. P. I. Balabanov and V. D. Filev, pp 42-46

This article examines the possibility of frequency-selective measurement of a complex alternating electrical voltage over the time of a signal by using a discrete

Fourier transform. Conditions for eliminating individual components, including the component caused by parasite pulse modulation, are derived on the basis of an analysis of the error sources. A way of ensuring a high measurement precision is shown. The main steps in the algorithm of the frequency-selective method of determining voltage are presented. An example of the use of the method developed to monitor the parameters of a telephone's signal with frequency sampling of the number of users is examined. Table 1, figure 1, references 3.

UDC 621.315:772.99

Kinoforms: Technologies, New Components, and Optical Systems. V. P. Korolkov, V. P. Koronkevich, I. A. Mikhaltsova, I. G. Palchikova, A. G. Poleshchuk, A. G. Sedukhin, A. P. Sokolov, Ye. G. Churchin, and Yu. I. Yurlov, pp 47-64

New optical components are proposed: a diffraction lens with an increased focal depth, a logarithmic axicon, a lensacon (lens + axicon), a diffraction fθ lens and modulated lenses for laser printers, an aspherical diffraction lens, and rasters with diffraction slits. The results of an experimental study of the aforementioned components are presented. The uses of diffraction elements in optic-oelectronic measuring devices are examined: a bifocal microscope, a laser slide wire, a playback head for a laser playback device, and an angle-code converter. Table 1, figures 19, references 20.

UDC 621.317

Sampled-Data Optical Mask-Type Fourier Processors. A. S. Blok and V. I. Yakovlev, pp 65-71

The design principles and main characteristics of sampled-data optical mask-type Fourier processors are examined. A classification system for them is proposed. It is shown that mask-type processors providing the same dynamic range as other optical processors with intensity modulation surpass the latter from the standpoint of precision of analysis, combining this advantage with simplicity of retuning the analysis band. Figures 3, references 7.

UDC 621.372.8:535.417

Structure of Induced Fields of Holographic Gratings in Planar Waveguide With Photogalvanic Write Mechanism. S. M. Shandarov, pp 72-77

Expressions are derived for induced fields in the initial write segment of holographic gratings in a planar waveguide formulated in a 3m symmetry crystal. The structure of the fields in the case where the grating written has different periods is calculated. Distributions of the amplitudes of induced perturbations of the tensor of the medium's dielectric permeability are presented. It is shown that holographic writing in a waveguide is caused by the components of the photogalvanic current directed both along the grating vector and along the normal to the waveguide surface. Figures 3, references 17.

UDC 616.07

Projection Algorithm for Smoothing and Differentiating Multidimensional Experimental Data. I. D. Grachev, M. Kh. Salakhov, and N. K. Shcherbakova, pp 78-81

An algorithm is developed. Its main idea is to use incompletely determined systems of linear equations while observing a non-negativity-type constraint and other analogous constraints. The iteration design of these equations gives a statistical regularized estimate of the solution being sought. Numerical experiments showing the efficiency and reliability of the proposed algorithm are conducted. Figures 3, references 12.

UDC 681.518.2:621.391

Precision of Assessing and Possibility of Discovering Failures in Filtration Systems With Redundancy of Measuring Systems. N. S. Demin and L. I. Luzina, pp 82-84

This article examines a linear sampled-data stochastic system with redundancy of the measuring systems in which, besides regular noise, anomalous noise caused by transducer failures are also active. Problems connected with the effect of the depth of redundancy on the precision of estimating and the capability of discovering failures are investigated. Several recommendations regarding the design of specific systems are given on the basis of the results obtained. References 10.

UDC 621.382.2

IR-Radiators With Barrier-Free Injection Mechanism. S. S. Bolgov, I. I. Golovach, V. N. Kabatsiy, V. K. Malyutenko, Z. I. Perchi, and Ye. I. Yablonskiy, pp 85-87

This article describes the design and most important parameters of a semiconductor infrared radiation source in the 3- to 7-μm range. Its operating principle is based on barrier-free "magnetic" charge carrier injection and negative luminescence. Unlike conventional lightguides, the radiating element does not have a p-n junction, it creates a positive or negative light contrast relative to the radiation background, it is effective under high-temperature conditions (T of 300 K or more), it is characterized by a high speed (τ of 10^{-8} s) and a significant IR radiation flux level (Δ of approximately 10^{-3} W/cm^2), and it may be used for optical information processing in an atmospheric window (3 to 5 μm) and in gas analysis instruments. Figures 4, references 5.

UDC 621.317.7

Investigation of Precision Characteristics of Two-Point Correlation Method of Measuring Frequency With Noise Compensation. N. P. Krasenko and V. A. Fedorov, pp 88-90

This article analyzes the precision characteristics of a two-point correlation method of measuring the frequency of a narrow-band steady random process with noise compensation in estimating the correlation function of a signal under investigation. The fundamental possibility of correct measurements of Doppler frequencies is shown, even for rather low signal-to-noise ratios with the required length of the implementation under investigation. Figure 1, references 2.

UDC 681.327.21

Error of Boundary Effects in Graphic Input Devices. V. I. Zhuravlev and V. P. Savenkov, pp 91-92

This article examines the reasons for read errors at the edges of the plotting board in graphic input induction devices. It includes an analysis of the signals' amplitudes along with the distribution and component of the error and approaches compensating for them. Figure 1, references 6.

UDC 681.3.06:519.17

Algorithm for Coloring Graph With Self-Learning. Ye. M. Kheyfets, pp 93-94

This article examines an algorithm for approximate solution of the problem of coloring the vertices of a finite nonoriented graph based on the use of an existing sequential algorithm and iterative reordering of the vertices based on the results of each step. The results of a computer experiment are presented. Figures 3, references 2.

UDC 621.391.837

Some Characteristic Features of Images in Primary Sections of Human Vision System. V. I. Gupal and I. V. Trokhimets, pp 95-97

This article proposes a refined model of the primary sections of the human vision system. The model makes an allowance for the defocusing of an image by the eye's crystalline lens, the nonlinear characteristic of the photoreceptors, and the phenomenon of lateral inhibition of the ganglion cells. It is shown that processing images in accordance with the given model results in the appearance of a function whose local extremes are located at the sites of the clusters of points where the glance is fixed when a person examines a given image. The location of the local extremes of the resultant function provides a good explanation of many geometric illusions inherent to the human vision system. Figures 3, references 6.

UDC 681.327

Interface Module for Information and Computing Systems Based on Elektronika 60 Microcomputer and DVK. Yu. A. Bunyak, N. M. Danilchuk, and Ya. I. Kapitskiy, pp 98-99

This article describes an interface module intended to connect hardware with different purposes to a type Elektronika 60 microcomputer and that performs the functions of exchanging data, sending files in a mode of direct access to memory, and interrupting of programs. It is based on series 1802 LSI microprocessor circuits and is located on the half-board of a microcomputer. Tables 2, figure 1, references 2.

UDC 621.317.79:535.317.1

Using Multielement Converters To Measure Distribution Functions. A. B. Katrich, pp 100-101

This article examines a method of determining the error in measuring the distribution functions of physical quantities. The need to allow for a priori information regarding a distribution to reduce the measurement error or to sample the dimensions of a multielement converter is shown. Figure 1, references 2.

UDC 621.398.1:681.2

Estimating Error of Even Approximation of Approximation Integrating Data Compression Algorithms. V. G. Lipskiy, pp 102-104

This article describes an approach to estimating the error of the even approximation of integrating data compression algorithms. Its use is shown by way of the example of the analysis of an existing algorithm. Results of an experimental investigation of the algorithm are presented. Figures 2, references 11.

UDC 629.7.018

Measuring Devices Based onActive Fiber-Optic Annular Structures. A. V. Loginov, M. Ya. Mesh, I. M. Ovchinnikov, V. V. Proklov, A. L. Shlifer, and G. A. Yudin, pp 105-106

This article examines the possibility of using active fiber-optic annular structures as base components of digital measuring devices. The feasibility of using the frequency of the turns of a pulse around an active fiber-optic annular structure as a signal parameter when measuring the magnitude of different effects resulting in a change in the length and refractive index of a fiber lightguide is explained. A temperature sensor based on an active fiber-optic annular structure is examined for an example. A method is proposed for increasing the sensor's sensitivity and linearizing its transfer function. The method is based on measuring the time in which a fixed number of pulse circulations around the active fiber-optic annular structure are completed. It is shown that highly sensitive measuring instruments with the functions of processing a signal all the way until the designated numbers are obtained are implemented on the basis of this method. Such instruments do not use analog signals and do not require analog-digital conversion. References 4.

UDC 681.327.68:778.38

Experimental Distribution of Power of Restored Images in Holographic Recording Devices. B. V. Vanyushev, pp 107-110

The distributions of the maximum power of the optical "0" and minimum power of the optical "1" in the restored image of a hologram given an approximation of the initial "1" and "0" array by independent, identically distributed random variables are examined on the basis of an asymptotic theory of extreme order statistics. Figures 2, references 7.

UDC 681.327.68:778.38

Distribution of Minima of Powers of "1" Images in Holographic Recording Devices. B. V. Vanyushev, pp 110-115

The distribution of the minimum of the powers of the optical "1" in the restored images of a holographic recording device is examined on the basis of a model of E_n sequences of random variables. The model investigated makes it possible to calculate the zone of the stable reading of holograms over a wide range of probabilities. Tables 2, figures 2, references 5.

END OF FICHE

DATE FILMED

1 MARCH 1990